

Learning Latent Variable Dynamic Models for Integrated Production Scheduling and Control

Calvin Tsay and Michael Baldea

McKetta Department of Chemical Engineering, The University of Texas at Austin
Austin, TX 78712

April 10, 2019

Abstract

With the increasing need for dynamic decisions in fast-changing markets, the integration of scheduling and control is an important consideration in chemical processes. Nevertheless, computing optimal production schedules with dynamic process models explicitly embedded remains challenging, due to their nonlinearity and high-dimensionality. In this paper, we observe that the intrinsic dimensionality of process dynamics (as relevant to scheduling) is often much lower than the number of variables. We introduce a data mining approach to learn closed-loop process dynamics on a low-dimensional, latent manifold. The manifold dimensionality is selected based on a tradeoff between model accuracy and complexity. After projecting process data, system identification and optimal scheduling calculations can be performed in the low-dimensional, latent space. We apply these concepts to schedule an air separation unit under model predictive control operating with time-varying electricity prices; our approach reduces the computational effort required while offering more detailed dynamic information compared to previous works.

Keywords: Integrated scheduling and control; nonlinear dimensionality reduction; autoencoders; system identification; air separation units

1 Introduction

The fast-changing conditions present in modern markets introduce many challenges and opportunities for improvements in chemical process operations. For example, partly due to increased adoption of intermittent renewable energy sources, electricity prices can fluctuate by several orders of magnitude during a 24-hour period. This provides a strong incentive for demand response, or intentional modification by an electricity user of its power consumption (“load shifting”) over time in order to exploit time-dependent electricity prices¹. In such circumstances, operational decision-making, namely, production scheduling, must be performed over relatively short time intervals to maximize profits. To ensure the resulting production schedules are feasible when implemented in the physical process, many research works and applications seek to integrate decision-making across different levels and time-scales, with a focus on accounting for process agility and process dynamics in scheduling calculations. Thus, the *integration of scheduling and control* for chemical processes has been identified as an important research area^{2;3;4;5}.

Scheduling refers to the determination of production sequences, product grades, batch sizes, unit assignments, and/or task timings that maximize profits (or minimize cost). Scheduling decisions are typically made over a time horizon on the order of hours to days. Most of the conventional methods for computing optimal schedules rely on the assumption that the process is at a steady state before and after each change in production targets. However, this assumption may not be valid when scheduling decisions are made over shortened time intervals, such as those required by

the aforementioned, fast-changing market conditions³. Many works have studied the interactions of chemical processes with the power grid^{6;7;8}, where, owing to market deregulation, electricity prices may change at hourly (or faster) time intervals; production scheduling decisions must therefore be made over a time scale in which process dynamics and control become highly relevant. Once the optimal schedule is determined, the control layer of a process seeks to track the setpoints/targets determined by the scheduling layer, while satisfying process and product constraints. To this end, optimization-based controllers (notably model predictive control–MPC) have become the standard advanced control approach in the chemical industry⁹. MPC determines the optimal control moves using a dynamic model that predicts the plant response (over a short prediction horizon) to changes in the manipulated variables.

In an early effort to integrate process scheduling and control, Flores-Tlacuahuac and Grossmann¹⁰ explicitly included the dynamic process model and controller in the scheduling problem, resulting in a large simultaneous dynamic optimization problem cast as a mixed-integer nonlinear program (MINLP). Zhuge and Ierapetritou¹¹ later implemented this discretized-time approach in a closed-loop strategy to mitigate effects of disturbances. Beal et al.¹² extended the discretized approach to allow for time-dependent parameters and constraints, while still accounting for the full dynamic process model, and the same group¹³ showed the economic benefits of integrated scheduling control in both open-loop and closed-loop implementations. Koller et al.¹⁴ considered embedding PI controllers into scheduling calculations in a stochastic framework that accounts for disturbances and uncertainties using a sample-based, back-off method. Many optimization techniques have been proposed to facilitate dealing with the integrated problem. Nyström et al.¹⁵ reduced the computational complexity of solving the integrated problem by decomposing it into a scheduling master problem and a control sub-problem, and iterating between the two. Nie et al.¹⁶ took a similar approach to develop a generalized Benders decomposition algorithm, where the scheduling decisions comprise the master problem and the dynamic process optimization comprises the primal problem. The decomposition approach was demonstrated with a large-scale integrated problem, where process dynamic models were again discretized in time and fully incorporated into a resource-task network scheduling problem. Simkoff and Baldea¹⁷ directly incorporated the KKT optimality conditions of a linear MPC system to provide an exact representation of closed-loop dynamics in the scheduling layer. The authors used a formulation with complementarity constraints to deal with the complementary slackness conditions associated with the MPC optimization problem.

For large-scale process models, computing optimal dynamic schedules can benefit from model reduction. Several works^{18;19} employed multiparametric model predictive control (mpMPC) in an optimal scheduling framework. Charitopoulos et al.²⁰ further examined the closed-loop implementation of an mpMPC approach for integrated scheduling and control that can handle dynamic disturbances. The mpMPC approaches generally rely on generating surrogate models for process dynamics and computing the control laws offline, but the problem complexity grows exponentially with the size of the control problem. As alternative means for model reduction, Cao et al.²¹ examined collocation-based dynamic models for an air separation unit, while Schäfer et al.²² proposed a compartmentalization-based model reduction technique. Du et al.²³ proposed representing the dynamics of a process and its controller using a low-order, input-output time scale-bridging model (SBM) in the scheduling layer. The authors employed input-output feedback linearizing controllers with integral action in order to impose simple closed-loop process dynamics amenable to the derivation of SBMs. In a similar vein, Baldea et al.²⁴ demonstrated the SBM approach for systems under MPC by designing a controller that imposes the desired simple closed-loop behavior.

Our recent work has investigated system identification as a means to create low-order models of process dynamics, which can then be embedded in optimal scheduling calculations. Dias et al.²⁵ integrated MPC in production scheduling calculations with low computational effort, by using sim-

ple state-space models of the *open-loop* process dynamics. The state-space models were derived via system identification from a series of open-loop step tests. An alternative approach is to perform system identification directly on the *closed-loop* process dynamics. Pattison et al.²⁶ introduced this idea using an air separation unit (ASU) application and showing that the computational time required for the integrated scheduling and control problem can be reduced by several orders of magnitude compared to using a first-principles (open-loop) dynamic model of the process. The same authors later included the approach in a moving horizon scheduling implementation²⁷. Kelley et al.²⁸ showed that the computational solution could be further expedited using a simultaneous approach with a fully-discretized time domain. Tsay et al.^{29;30} applied the framework to an industrial ASU operating under MPC; system identification was performed using readily available historical operating data without deliberate excitation (e.g., step tests).

In this work, we present a novel scheduling framework that accounts for closed-loop process dynamics using a low-dimensional, latent-variable representation. We first analyze the intrinsic low-dimensionality, or approximate low-dimensionality, of closed-loop process dynamics relevant to scheduling. This observation motivates learning the underlying *latent manifold* that describes the process behavior in its intrinsic dimension, as well as using a low-dimensional representation of closed-loop process dynamics in scheduling calculations. The novelty of this contribution consists of the following:

- A conceptual approach for identifying a low-dimensional manifold underlying closed-loop process behavior using standard data-mining techniques. We further show that autoencoders provide a simple method to learn both linear and nonlinear relationships among process variables.
- A framework for system identification in the space of the learned latent variables. In contrast to previous works^{26;29;30} that rely on manually selecting a subset of “scheduling-relevant” variables from often high-dimensional process state and output vectors, the present framework automates the dimensionality-reduction process, eliminating the need to heuristically decide *a priori* which process constraints may be active during scheduled transitions.
- A methodology for integrated scheduling and control using the above low-dimensional representation of closed-loop process dynamics. Owing to its low intrinsic dimensionality, the resulting problem exhibits reduced computational complexity, while retaining the relevant process dynamics.

We apply the proposed approach to derive data-driven, latent-variable models of an air separation unit (ASU) considered in previous works^{26;25}. Furthermore, we demonstrate that the proposed framework allows for computationally efficient integrated scheduling and control calculations of the ASU in a demand-response scenario with hourly electricity prices. Finally, we investigate tuning the dimensionality of the reduced-order representation (i.e., selecting the number of latent variables) to manage the tradeoff between optimization problem size and model accuracy.

2 Background

2.1 Integrated Scheduling and Control Problem

The integrated scheduling and control problem aims to include the *closed-loop* dynamics of a process in the production scheduling problem. The deterministic, continuous-time integrated

scheduling and control problem can be stated generally as²³:

$$\max_{\mathbf{y}_{sp}(t)} \int_{t=0}^{t=t_f} P(\mathbf{y}, t) dt \quad (1)$$

$$s.t. \quad \dot{\mathbf{x}} = f(\mathbf{x}) + G(\mathbf{x})\mathbf{u} \quad (2)$$

$$\mathbf{y} = h(\mathbf{x}) \quad (3)$$

$$\mathbf{u} = K(\mathbf{y}_{sp} - \mathbf{y}) \quad (4)$$

$$l(\mathbf{x}, \mathbf{y}, \mathbf{u}, t) = 0 \quad (5)$$

$$\begin{bmatrix} \mathbf{x}^L \\ \mathbf{y}^L \\ \mathbf{u}^L \end{bmatrix} \leq \begin{bmatrix} \mathbf{x} \\ \mathbf{y} \\ \mathbf{u} \end{bmatrix} \leq \begin{bmatrix} \mathbf{x}^U \\ \mathbf{y}^U \\ \mathbf{u}^U \end{bmatrix} \quad (6)$$

where $\mathbf{y}_{sp}(t)$ is a time-varying vector of production targets and/or other setpoints to be supplied to the control system, and K represents the process control policy. The vector $\mathbf{x} \in \mathbb{R}^n$ denotes the process state variables, $\mathbf{y} \in \mathbb{R}^m$ are the output variables, $\mathbf{u} \in \mathbb{R}^u$ are the input variables, f and h are appropriately defined vector fields, and G is of appropriate dimensions. The process variables $\mathbf{x}, \mathbf{y}, \mathbf{u}$ may be subject to constraints, given by (6). The economic objective function $P(\mathbf{y}, t)$ typically includes the revenue from selling product, and the process operating costs. $l(\cdot)$ includes storage and demand constraints that ensure (i) customer demand can be met at all times, (ii) the amount of product stored does not deplete/exceed the physical capacity of the storage system, and (iii) artificial economic gains are not realized by depleting material hold-up present at $t = 0$. Note that $l(\cdot)$ may include both path and endpoint constraints.

2.2 Scale-Bridging Models

Theoretical developments^{24;31} have shown that the closed-loop, input-output dynamic behavior of process systems (i.e., the response of the process to changes in \mathbf{y}_{sp}) may be quite slow in comparison to the evolution of states of the individual process units. The former, input-output behavior often evolves over time scales relevant to process scheduling calculations, particularly in the context of the fast-changing market conditions described earlier. Moreover, these results^{24;31} suggest that the input-output dynamic behavior can be described, or well-approximated, using a low-dimensional model. On this basis, our previous works proposed representing the process dynamics in scheduling calculations using time scale-bridging models (SBMs), which are a low-order representation of the closed-loop dynamics of the process. Broadly speaking, low-order SBMs can be derived using either model reduction or system identification, and the two techniques are briefly reviewed below:

- **Model reduction** refers to systematic derivation of a low-order model from a detailed (high-dimensional and likely first-principles) dynamic process model. Many methods have been proposed for systematic model reduction, such as asymptotic analyses^{31;32} or null-space projection³³. These methods reduce the number of states, typically in systems that exhibit multiple time scale dynamics, resulting in a lower-dimensional DAE system. These modeling techniques retain physically meaningful states, which can be a useful feature for controller design and monitoring strategies^{31;34}. Alternative techniques such as empirical Gramians³⁵ and proper orthogonal decomposition^{36;37} can also be used, although these methods can result in states that are not physically meaningful.
- **System identification**, the second category, refers to “learning” a dynamic model from process operating data. In this approach, a full-order, dynamic process model is not required. Rather, a generic model structure is assumed, and its parameters are computed based on tran-

sient data recorded from the process. The data can be generated in the course of the (routine) operation of a physical process or from simulations of a detailed and accurate mathematical model. Learning (and reducing the dimensionality of) dynamics from data is a highly active area of research³⁸. We direct the interested reader to, e.g., the book by Zhu³⁹ for an overview of the multitude of available system identification techniques.

Our recent works^{26;29;30} have focused on system identification methods for building SBMs and SBM-based scheduling. Pattison et al.²⁶ suggested that the dimensionality (and consequently the computational complexity) of the scheduling problem (1)–(6) could be considerably reduced by restricting modeling efforts to “scheduling-relevant variables.” In this approach, a subset $\mathbf{z} \subseteq [\mathbf{x}, \mathbf{y}, \mathbf{u}]$ is defined, that includes the input and output variables (\mathbf{u} and \mathbf{y}) that affect $P(\cdot)$ and $l(\cdot)$. Process state and output variables (\mathbf{x} and \mathbf{y}) whose constraints are active during steady-state operation or during process transitions are said to limit the process “dynamic agility” and are also included in \mathbf{z} to ensure that the resulting schedules do not violate any constraints during transitions or production periods (i.e., guarantee the dynamic feasibility of a schedule). In essence, the dimensionality reduction occurs through a manual, heuristic selection of the scheduling-relevant variables $\hat{\mathbf{x}} \subseteq \hat{\mathbf{x}}$, $\hat{\mathbf{y}} \subseteq \hat{\mathbf{y}}$, and $\hat{\mathbf{u}} \subseteq \hat{\mathbf{u}}$. The resulting scheduling optimization problem is similar to (1)–(6), but can contain significantly fewer variables and constraints:

$$\max_{\mathbf{y}_{sp}} \int_{t=0}^{t=t_f} P(\mathbf{z}, t) dt \quad (7)$$

$$s.t. \quad \dot{\mathbf{z}} = \begin{bmatrix} \dot{\hat{\mathbf{y}}} \\ \dot{\hat{\mathbf{x}}} \\ \dot{\hat{\mathbf{u}}} \end{bmatrix} = \hat{f}(\mathbf{z}, \mathbf{y}_{sp}) \quad (8)$$

$$l(\mathbf{z}, t) = 0 \quad (9)$$

$$\mathbf{z}^L \leq \mathbf{z} \leq \mathbf{z}^U \quad (10)$$

where $l(\mathbf{z}, t)$ may include both path and endpoint storage/demand constraints. The reduced-space dynamic model $\hat{f}(\mathbf{z}, \mathbf{y}_{sp})$ represents the scale-bridging model (SBM), which describes the input-output relationship between the process setpoints and the scheduling-relevant variables and replaces the dynamic models present in (1)–(6).

2.3 Manifold Learning

While limiting the scheduling problem to only consider the dynamics of “scheduling-relevant variables” can be an effective form of dimensionality reduction, the partitioning of variables relies on manual effort, technical insight, and human expertise. On the other hand, chemical processes typically have many sensors that record process variables at frequencies in the order of minutes, generating “big data” sets that can be exploited to understand the underlying system behavior. There exist many approaches for learning low-dimensional representations of a dynamical system from recorded data. In this context, *manifold learning* refers to identifying a low-dimensional manifold on which higher-dimensional data points intrinsically lie. The learned manifold represents a subspace of the full-dimensional variable space that explains (most of) the variation observed in the data set. Observations of the original system can be transformed to a smaller set of *latent variables* that parameterize the manifold.

A broad class of unsupervised machine learning algorithms can be applied to the task of manifold learning. Pearson⁴⁰ introduced principal component analysis (PCA) in 1901, and the technique is now a widely accepted dimensionality-reduction technique. PCA consists of finding a linear coordinate transformation whereby the data are projected on a new set of latent variables. The coordinate transform is constructed such that the amount of variance captured by each successive

latent variable, or principal component, is maximized. Latent variables based on linear combinations of the original variables, such as those from PCA, are commonly used in the process industries for process monitoring and troubleshooting⁴¹. They have also found applications in process control, where they can be employed to reduce the dimension of the controlled variable space. For example, the latent variables can replace the original process controlled variables to simplify controller calculations^{42;43}.

While PCA is limited to finding linear mappings, a number of nonlinear manifold learning algorithms have been presented. A simple nonlinear extension of PCA is kernel PCA, where a nonlinear kernel is first applied, and PCA is performed in the processed feature space⁴⁴. Several researchers have studied the relationships between PCA and a particular class of artificial neural network known as autoencoders. Of particular note, Sanger⁴⁵ showed that linear autoencoders correspond exactly to PCA, while Kramer⁴⁶ proposed nonlinear autoencoders as a form of generic, nonlinear PCA. Many other nonlinear manifold learning techniques have been since proposed, including diffusion maps⁴⁷, Laplacian eigenmaps⁴⁸, locally linear embeddings⁴⁹, stochastic neighbor embeddings (SNE)⁵⁰, and Isomap⁵¹. For further details, the reader is referred to the book by Lee and Verleysen⁵² and the review by Van Der Maaten et al.⁵³.

3 Scheduling with Learned Latent Variables

3.1 Concept

We observe now that the *intrinsic dimensionality*, or the number of independent variables underlying the significant nonrandom variations in the observations, of the closed-loop behavior of an entire chemical process can be much lower than the apparent *extrinsic dimensionality* of the process ($n + m + u$). In particular, the dimensionality of the process input \mathbf{u} , output \mathbf{y} , and state \mathbf{x} variables can be related to just the process state variables \mathbf{x} :

$$\mathbf{x}^* \equiv \begin{bmatrix} \mathbf{x} \\ \mathbf{y} \\ \mathbf{u} \end{bmatrix} = \begin{bmatrix} \mathbf{x} \\ h(\mathbf{x}) \\ K(\mathbf{y}_{sp} - h(\mathbf{x})) \end{bmatrix} \quad (11)$$

where we define the augmented process state variable vector \mathbf{x}^* as $[\mathbf{x}, \mathbf{y}, \mathbf{u}]$. Therefore, the mapping from the schedule-defined setpoints \mathbf{y}_{sp} to the process variables $[\mathbf{x}, \mathbf{y}, \mathbf{u}]$ has an intrinsic dimensionality equal to $\dim_i(\mathbf{x})$. We use $\dim(\cdot)$ to denote extrinsic dimensionality and $\dim_i(\cdot)$ to denote the intrinsic dimensionality, as defined above. Note that this assumes $\mathbf{u} = K(\mathbf{y}_{sp} - h(\mathbf{x}))$ can be evaluated directly, or an explicit control law exists. In the case of an implicit/optimization-based controller, an explicit relationship may still exist, or an approximation may be possible⁵⁴. We shall examine the case of dimensionality reduction for a process operating under an optimization-based controller in the case study below.

Regarding the control policy, Lovelett et al.⁵⁵ observed that, for a system operating under MPC, the optimal control policy \mathbf{u} may have a significantly lower *intrinsic* dimensionality than its *extrinsic* dimensionality. The extrinsic dimensionality of \mathbf{u} is equal to $N \times \dim(\mathbf{u})$, where N is the number of computed steps. However, the intrinsic dimensionality is limited by $\dim_i(\mathbf{u}) \leq \dim(\mathbf{y}) + \dim(\mathbf{y}_{sp}(t))$. Here, \mathbf{y} represents the vector of current values of the output variables and $\mathbf{y}_{sp}(t)$ represents the reference trajectory. Note that $\dim(\mathbf{y}_{sp}(t))$ is dependent on the parameterization of $\mathbf{y}_{sp}(t)$ with respect to time. Importantly, the intrinsic dimensionality of the control policy $\dim_i(\mathbf{u})$ is often lower than this limit. This may occur for many reasons, including a system whose dynamics lie on a low-dimensional, slow manifold³¹, or whose state-space realization is non-minimal order (containing redundant information⁵⁵). We exploited the former phenomenon in our previous works^{23;26} to describe the scheduling-relevant dynamics of \mathbf{z} as a function of $\mathbf{y}_{sp}(t)$ using low-order SBMs.

In this work, we propose a new learning-based approach for low-order SBM generation, whereby we find a combined latent manifold mapping of the full augmented process state variable vector \mathbf{x}^* . We desire an invertible mapping $\mathbf{x}^* \leftrightarrow \phi$, with $\phi \in \mathbb{R}^p$, denoted as $\phi = c(\mathbf{x}^*)$ and $\mathbf{x}^* = c^{inv}(\phi)$. Furthermore we desire to identify the mapping $c : \mathbb{R}^n \times \mathbb{R}^m \times \mathbb{R}^u \rightarrow \mathbb{R}^p$ such that $p \ll n + m + u$. We note that such a mapping always exists for $p \leq n + m + u$, since a trivial exact mapping is possible at $dim(\phi) = dim(\mathbf{x}^*)$. Once a mapping is identified, the dynamics of the *latent variables* ϕ can be embedded in the scheduling problem. The resulting scheduling problem has a low intrinsic dimensionality, with dynamics evolving only in the (low-dimensional) latent-variable space \mathbb{R}^p :

$$\max_{\mathbf{y}_{sp}} \int_{t=0}^{t=t_f} P(\mathbf{y}, t) dt \quad (12)$$

$$s.t. \quad \dot{\phi} = f^\phi(\phi, \mathbf{y}_{sp}) \quad (13)$$

$$\mathbf{x}^* \equiv \begin{bmatrix} \mathbf{x} \\ \mathbf{y} \\ \mathbf{u} \end{bmatrix} = c^{inv}(\phi) \quad (14)$$

$$l(\mathbf{x}^*, t) = 0 \quad (15)$$

$$\mathbf{x}^{*L} \leq \mathbf{x}^* \leq \mathbf{x}^{*U} \quad (16)$$

Assuming that the mapping $c : \mathbf{x} \rightarrow \phi$ and the inverse mapping $c^{inv} : \phi \rightarrow \mathbf{x}$ exist, the dimensionality of the dynamic constraint(s) is now $p = dim(\phi)$. Furthermore, if the mappings $c(\cdot)$, $c^{inv}(\cdot)$ are exact, and the dynamics of the latent variables are represented accurately by $f^\phi(\cdot)$, the scheduling problem in (12)–(16) is identical to the original scheduling problem in (1)–(6). Note that for $c(\cdot)$, $c^{inv}(\cdot)$ to be exact, or equivalently, $c^{inv}(c(\mathbf{x}^*)) = \mathbf{x}^*$, \mathbf{x}^* can only contain p independent variables. The remaining variables must be (nonlinearly) correlated. In practical situations, process variables that feature path constraints of the type in (16) may only be a subset of the full vector of process variables, and manifold learning can be carried out in a space of already lower dimension. Importantly, recent work^{56;57} has highlighted tradeoffs between dynamic production schedules and equipment fatigue. To account for this, some variables without explicit constraints may still be relevant in the scheduling layer and should be included in \mathbf{x}^* .

If the dynamics of \mathbf{x}^* present a low-dimensional manifold only in a limit case (e.g., when the process dynamics are in a singularly perturbed form), the low-dimensional dynamics only approximate the true system. Specifically, when the mappings $c(\cdot)$, $c^{inv}(\cdot)$ are inexact, then $c^{inv}(c(\mathbf{x}^*)) \approx \mathbf{x}^*$. Some information may be lost by “collapsing” the dynamics of \mathbf{x}^* onto a reduced dimension, resulting in an approximation we denote as $\mathbf{x}^{*'} = c^{inv}(c(\mathbf{x}^*))$. The accuracy of the approximation, in terms of $\|\mathbf{x}^* - \mathbf{x}^{*'}\|$ can be improved by increasing p until the original system is fully recovered at $p = n + m + u$ (or lower if some variables are correlated). In other words, the dimension of the latent manifold p can be used as a parameter for adjusting the accuracy of the reduced-order representation of the closed-loop dynamics.

Remark 1. *Reducing the number of dynamic variables from (7)–(10) to (12)–(16) may be beneficial for both sequential³⁰ and simultaneous²⁸ dynamic optimization approaches. In this work, we focus on sequential approaches, where the Jacobian size for computing implicit time integration steps is reduced by limiting the number of dynamic variables to p . We expect the benefits to also extend to simultaneous approaches, where the number of differential state variables treated by the optimization problem is still reduced. However, note that the explicit dimensionality of $dim(\mathbf{x}^*)$ may remain larger than in (7)–(10). We refer the interested reader to^{58;59} for an overview of sequential techniques for dynamic optimization and⁶⁰ for information on simultaneous strategies.*

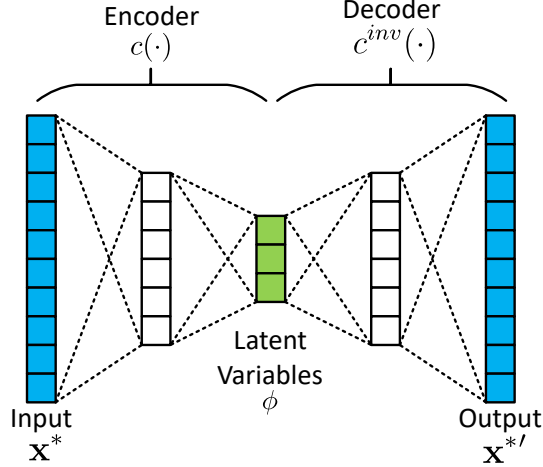


Figure 1: Conceptual depiction of an undercomplete autoencoder.

3.2 Latent Variable Scheduling Framework

The proposed approach for latent variable scheduling comprises the following steps:

1. Obtain historical process operating data representative of typical production schedules
2. Learn latent variable mappings $c : \mathbf{x}^* \rightarrow \phi$ and $c^{inv} : \phi \rightarrow \mathbf{x}^{*'}$
3. Transform historical data $\mathbf{x}^*(t)$ using c to produce $\phi(t)$
4. Determine model form and fit a dynamic model to the latent variables $\dot{\phi} = f^\phi(\phi, \mathbf{y}_{sp})$ using the transformed data set
5. Solve low-dimensional scheduling problem (12)–(16) with path constraints on $\mathbf{x}^{*'} = c^{inv}(\phi)$

3.3 Learning Latent Variables with Autoencoders

Autoencoders (AEs) provide a straightforward means for manifold learning, since they can simultaneously learn a complex (nonlinear) mapping $c(\mathbf{x}^*)$ and an associated inverse mapping $c^{inv}(\phi)$ using simple basis functions. Linear autoencoders operate in the same space as PCA⁶¹, while Kramer⁴⁶ demonstrated the effectiveness of nonlinear autoencoders as a form of nonlinear PCA. A brief overview of the technique as relevant to the current work is presented here; the interested reader is referred to Chapter 14 of the book by Goodfellow et al.⁶¹ for a discussion of autoencoders, their uses, and comparisons to other manifold learning techniques.

Briefly speaking, an *autoencoder* is a particular type of feed-forward artificial neural network that aims to replicate its input at its output. At a particular hidden layer within the autoencoder, the input is described as a “code”, or ϕ . The dimensionality of the code ϕ is determined by the structure of the neural network. The full network comprises $(c^{inv} \circ c)(\mathbf{x}^*)$. The autoencoder is naturally split into the layers leading to ϕ , or $\phi = c(\mathbf{x}^*)$, and the subsequent layers, or $\mathbf{x}^{*'} = c^{inv}(\phi)$. The output of the network, $\mathbf{x}^{*'} = c^{inv}(c(\mathbf{x}^*))$ is an estimate of the original input \mathbf{x}^* . The autoencoder is typically trained using an iterative method by minimizing a loss function L ,

$$L(\mathbf{x}^*, \mathbf{x}^{*'} = c^{inv}(c(\mathbf{x}^*))) \quad (17)$$

which penalizes discrepancies between $\mathbf{x}^{*'}$ and \mathbf{x}^* . Commonly used loss functions include the mean squared error, mean absolute error, and variations of the hinge and cross-entropy functions.

For the purpose of learning a low-dimensional manifold underlying input data, we are particularly interested in *undercomplete autoencoders*, or those with ϕ constrained to have a lower dimension than \mathbf{x}^* . By restricting, or “bottlenecking”, information flow through the feed-forward neural network, undercomplete autoencoders can generally capture the salient trends present in the training data. Figure 1 depicts a simple undercomplete autoencoder with a two-layer encoder, two-layer decoder, and an encoded dimensionality of three. Undercomplete autoencoders are often constructed with an encoder and decoder that each comprise a single hidden layer. The universal approximator theorem⁶² guarantees that a feedforward neural network with at least one hidden layer can approximate any function (within a broad class) to an arbitrary degree of accuracy, given that enough hidden units are present. In practice, however, autoencoders with multiple hidden layers (termed *deep* autoencoders) can sometimes reduce the computational cost of representing certain functions, improve data compression, and/or decrease the amount of training data required^{61;63}. Thus, with enough hidden units through depth or breadth, any (nonlinear) mapping between $\mathbf{y} = h(\mathbf{x})$ and $\mathbf{u} = K(\mathbf{y}_{sp} - h(\mathbf{x}))$ as relevant to the dynamical system under consideration here can be modeled to arbitrary accuracy, provided that $K(\cdot)$ is bounded and continuous. Note that MPC may not always satisfy this property, and alternative manifold learning techniques may be more suitable for systems exhibiting many discontinuous operating regimes.

3.4 Building Latent Variable SBMs

After a latent manifold underlying the closed-loop dynamics of a process is learned, the process operating data can be projected to the latent manifold to produce a low-dimensional representation. In particular, each observation $\mathbf{x}^*(t)$ can be transformed to $\phi(t) = c(\mathbf{x}^*(t))$. Then, given a data set (e.g., the data set used for manifold learning) of transformed observations $\phi(t)$ and process setpoints $\mathbf{y}_{sp}(t)$, we can perform system identification in the latent variable space to create a data-driven, scale-bridging model (SBM) of the low-dimensional process dynamics, $\dot{\phi} = f^\phi(\phi, \mathbf{y}_{sp})$. For system identification, the choice of the functional form of dynamic model can be arbitrary. The dynamics of the latent variables underlie the dynamics of the system variables \mathbf{x}^* , and an initial attempt may involve model forms that adequately represent the dynamics of $\mathbf{x}^*(t)$. The system identification step can introduce additional inaccuracy in the dynamics embedded in the latent variable scheduling problem (12)–(16); however, this is equally true when identifying SBMs using actual process variables, as used in (7)–(10)^{26;30}. The identification of accurate dynamic models is a crucial step in both data-driven approaches.

Our previous works^{26;30} employed SBMs in the Hammerstein-Wiener (HW) form to capture the closed-loop process dynamics of actual, physical process variables for scheduling applications. This choice was motivated by the inherent structure of HW models. In contrast to unstructured models (e.g., the recurrent neural networks described in Chapter 10 of⁶¹), HW models have fewer parameters to regress and can be trained with significantly lower amounts of data. This is an important feature, since system identification experiments in chemical plants can be expensive and time-consuming. A HW model comprises a linear dynamic component flanked by static, nonlinear input and output transformations. A single-input single-output (SISO) HW model can be written with the linear dynamic component represented as a state-space model:

$$h = H(y_{sp}) \tag{18}$$

$$\dot{\vec{r}} = A\vec{r} + Bh \tag{19}$$

$$w = C\vec{r} \tag{20}$$

$$\mathbf{x}^* = W(w) \tag{21}$$

where H and W are, respectively, the Hammerstein and Wiener blocks corresponding to the static,

nonlinear input and output transformations. A , B , and C are the matrices defining the linear state-space dynamical system, which is of order n_d , with $\vec{r} \in \mathbb{R}^{n_d}$. The SISO model in (18)–(21) is written for a single model input y_{sp} and a single model output x^* .

The order of the linear dynamics and the choice of nonlinear transformations represent structural decisions that can also be made based on the data, such as by employing some information criterion³⁰. Typical nonlinear transformations for H and W include piecewise linear functions, sigmoid networks, saturation functions, or polynomials⁶⁴. Once the order of the linear state-space system and the nonlinear transformations are determined, the parameters of the H , W , and the dynamical system are typically fitted simultaneously to a training data set using an iterative solver. For systems with multiple production setpoints, a multi-input, single-output (MISO), HW model can be identified for each system output³⁰. Since HW models were successfully applied in previous works and can be trained with relatively small data sets, we employ HW models to model the dynamics of latent variables in this work. The selection of HW models for this study also facilitates comparison of system identification and scheduling results to related works^{26;27;28;25;29;30} involving data-driven models of HW form.

4 Case Study: Demand-Response Scheduling of an Air Separation Unit

4.1 Description of ASU Process

Many works have considered the optimal scheduling of cryogenic air separation units (ASUs): due to their large electricity consumption, ASUs can derive significant economic benefits from scheduling production in response to time-varying electricity prices (demand response). A common approach for scheduling ASUs is to assume quasi-stationary operation and use additional constraints to reflect the transition capabilities of the plant^{1;65}; a few recent examples are reviewed here. Zhang et al.⁶⁵ employed a mode-based scheduling framework with surrogate sub-process models for computationally efficient scheduling calculations. Similarly, Zhou et al.⁶⁶ defined a set of operational modes from historical data and used associated convex hulls for schedule optimization. More recently, Zhao et al.⁶⁷ proposed a state-transition network model for scheduling ASUs, and applied it to a large-scale scheduling problem including two multi-product ASUs. Obermeier et al.⁵⁶ defined a mode-based scheduling approach to examine the important relationship between DR scheduling and equipment fatigue.

In this work, we consider the single-product ASU process shown in Figure 2. The detailed mathematical model of the process dynamics is based on the work of Cao et al.⁶⁸, and is presented in full by Johansson⁶⁹. Pattison et al.²⁶ investigated the scheduling problem using the full-order, detailed process model (1)–(6), as well as the reduced-order SBM scheduling problem (7)–(10). Dias et al.²⁵ developed a MPC system for the process and applied a novel simulation-optimization framework for integrated scheduling and control including MPC. Here, we employ the MPC system and its associated state-space models given by Dias et al.²⁵ with slight modification. The mathematical model of the process and its control system are summarized below.

The process in Figure 2 produces high-purity nitrogen from an inlet air feed stream. The feed stream is compressed from atmospheric pressure to 6.8 bar, cooled, and passed through a primary (multi-stream) heat exchanger (PHX) against warming cryogenic streams. A portion of the air is removed from the PHX at an intermediate point and is sent to a turbine to generate electricity; the remainder exits the PHX at its saturation point. The two streams are combined and sent to the bottom of a cryogenic distillation column, which separates nitrogen from the other components of air. The bottoms product of the column is expanded through a valve before entering the reboiler. The reboiler and condenser are integrated in a single unit, allowing the bottoms stream to provide cooling duty to the condenser. The distillate of the column comprises the desired high-purity nitrogen stream. A portion of the distillate is sent to the condenser and refluxed to the column,

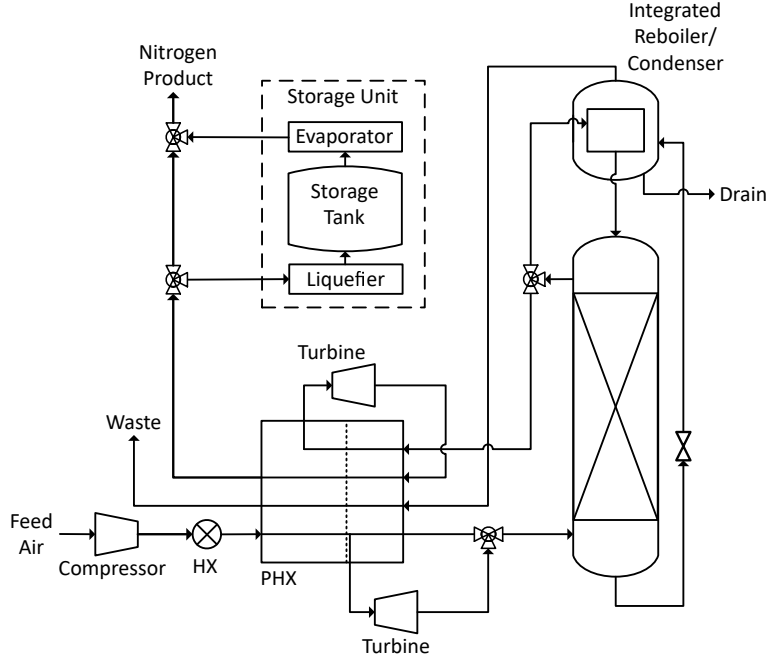


Figure 2: Flowsheet for a small nitrogen-production ASU with liquefier and liquid storage capacity.

while the remaining product stream is expanded in a second turbine after being vaporized in the PHX. The product stream and the waste nitrogen stream from the reboiler both pass through the PHX to provide cooling duty to the incoming air. The nitrogen liquefier, storage, and evaporator units are included in the flowsheet. These units allow the plant to liquefy and store extra gaseous nitrogen during times of over-production, and conversely evaporate stored liquid nitrogen to satisfy gas nitrogen demand during times of under-production.

The process model comprises 6,094 equations and has 430 differential variables. The entire model is implemented in gPROMS, and implementation details can be found in our previous works^{25;26}. The ASU process is assumed to operate with a constant gas nitrogen demand of 20 mol/s, with less than 2000 ppm impurity (oxygen and argon). The process is assumed to be able to modulate its production rate by $\pm 20\%$ from its nominal value, representing a production range of 16 mol/s to 24 mol/s. The MPC for the process has four controlled variables and three manipulated variables. While the liquid drain in the reboiler was previously used as a fourth manipulated variable²⁵, we found that outputs are not sensitive to this input in the desired range of operation. The MPC variables are summarized in Table 1. The MPC has a sample time of six minutes and employs a linear state-space model created from system identification tests on the full-order dynamic model. The production rate setpoint represents $\mathbf{y}_{sp}(t)$, and its time-dependent value is set by the solution to the scheduling problem. The setpoints for the remaining controlled variables are fixed at $I_p^{sp} = 500$ ppm, $\Delta T_{IRC}^{sp} = 2.2$ K, and $M_{reb}^{sp} = 100$ kmol. The MPC was implemented in MATLAB using the Model Predictive Control Toolbox.

4.2 Simulation for Generating Training and Testing Data

The augmented state variable vector for scheduling the ASU comprises 15 variables, i.e., $\dim(\mathbf{x}^*) = 15$: the seven variables of the MPC (Table 1), the power consumption, and seven state variables that feature constraints. These are the storage level M_{store} , column weeping ratio, column flooding ratio, column sump level, bubble-point pressure ratio, dew-point pressure ratio, nitrogen pressure ratio. The bubble-point pressure ratio, defined as the ratio of pressure to bubble-point pressure

Controlled Variable y_p	Manipulated Variable u_p
Production flow rate	Inlet air flow rate
Product impurity	PHX split fraction
IRC temperature difference	Vapor product split
Reboiler liquid level	

Table 1: Summary of MPC variables for the ASU Process

for the stream exiting the PHX must be greater than one to ensure the stream is fully liquefied. The dew-point and nitrogen point pressure ratios, defined as the ratio of pressure to dew-point pressure for, respectively, the feed stream drawn at an intermediate location in the PHX and the product stream passing through the turbine, must be less than one to ensure the streams are fully vapor-phase. Note that \mathbf{x}^* contains several each of input variables, state variables, and output variables. A full list of the variables included in \mathbf{x}^* is provided in the Appendix.

Pattison et al.²⁶ found that several of these constraints are inactive at steady state and during transitions in a small training data set; therefore, the authors only considered eight SBMs. Dias et al.²⁵ modeled only the variables involved in the MPC, the power consumption, and the storage level. The remaining process states were assumed to not affect schedule feasibility. The variables for which dynamic SBMs were derived in the two referenced works are also listed in the Appendix. While the manipulated variables are not subjected to path constraints, it is important to consider them at the scheduling layer to understand the degree to which modulating plant operations is possible and potential effects on the equipment^{56;57}.

A data set was simulated for manifold learning using the detailed first-principles process model described by Johansson⁶⁹. The MPC was implemented “online” by linking the full-order dynamic model with the Model Predictive Control Toolbox in MATLAB. The full-order model was run between each MPC interval to generate sampled state variable values, and the MPC was solved in MATLAB to provide updated setpoints for the local regulatory controller in the subsequent interval. To generate an operating data set that reflects production modulation, the SBM-based scheduling problem (7)–(10) was solved using two-day electricity price data from a regional independent service operator (ISO). Ten such two-day price signals were selected, aiming to include a wide gamut of process closed-loop behaviors. In total, 20 days of operating data were included in the data set. The electricity prices and resulting production targets used to generate the data set are shown in Figure 3. Static dimensionality reduction techniques were applied to the simulated data set, and their statistics, as presented below, were computed using 5-fold cross-validation.

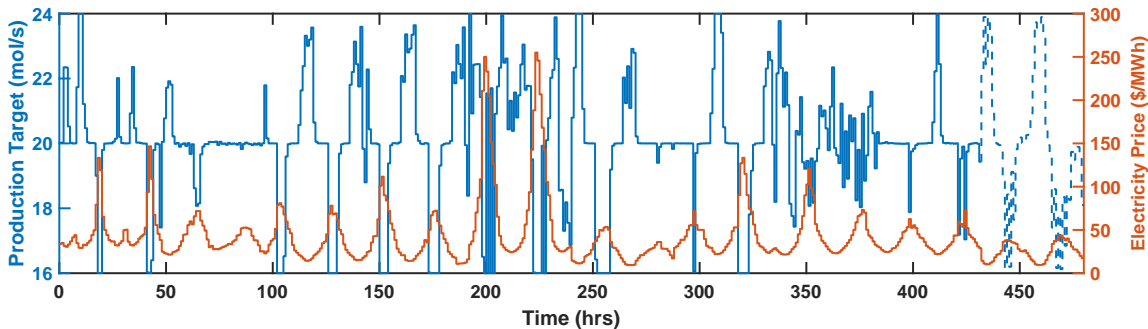


Figure 3: Electricity prices and production setpoints used to generate data set. The dashed lines depict the last 10% of the data, which are used for dynamic model validation.

Principal component analysis (PCA) reveals the linear relationships and correlations present in \mathbf{x}^* in the data set. The percentage of variance explained by each principal component for the full data set is shown in Figure 4. To ensure the correlation indicated by PCA is not coincidental, the same analysis was applied to the case where \mathbf{x}^* included all *process-level* variables. Here, the set of process-level variables refers to the properties of inter-unit streams (i.e., temperature, pressure, composition) and the operating conditions of the process units. Excluding variables that are necessarily identical to others and those with fixed/set values, there are 70 process-wide variables in total. Note that while the full dynamic model includes 6,094 equations, we limited this analysis to process-level variables, which provide ample information for most scheduling calculations.

PCA of the full data set produced a similar result to the case of 15 variables. In both cases, the percentage of variance explained decreases quickly with an increasing number of principal components (note the logarithmic ordinate scaling in Figure 4), suggesting that the closed-loop process dynamics of \mathbf{x}^* can be “collapsed” to a lower dimension, and that the accuracy of the approximation can be tuned by carefully selecting the dimensionality of the reduced-order representation. The variance captured decays more slowly after approximately 12 components for the case of all process-wide variables, since only the first 15 components (of 70) are shown.

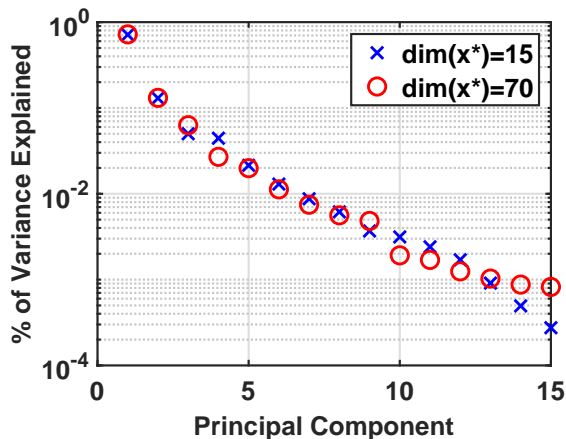


Figure 4: Percentage of variance in the full data set explained by each principal component.

4.3 Manifold Learning Results

Though PCA showed that the data set could be approximated reasonably using a low-dimensional set of linear latent variables, we incorporate nonlinear manifold learning techniques to further capture nonlinear correlations in the closed-loop process dynamics. Manifold learning on the data set was performed using autoencoders (AEs). Several AE architectures were tested: $Tanh(2x)$, having \tanh activation functions and one hidden layer in the encoder and decoder; $Tanh(3x)$, having \tanh activation functions with two hidden layers in the encoder and decoder; and $Linear$, with linear activation functions. As mentioned above, the representation power of an AE can be increased through increasing the depth or breadth of the neural network. In this study, the breadth of hidden layers is fixed to the truncated average of the input dimension and the encoded dimension. The effect of increasing the network size is investigated by switching from a single hidden layer to two hidden layers. Note that adding hidden layers to a neural network with only linear transformations does not increase the representation power of the model, since linear combinations of linear basis functions remain linear.

Each process variable was scaled to take values between 0-100%, with 0% representing its minimum value in the data set and 100% representing its maximum. The AEs were implemented

and trained using TensorFlow⁷⁰ with the Adam solver⁷¹ and the mean squared error (MSE) as the loss function:

$$\text{MSE} = \frac{\|x_{ref} - x\|^2}{N_s} \quad (22)$$

where N_s is the number of samples. Each AE was trained until the validation loss function remained the same or increased for several straight epochs. The cross-validated test MSEs from training the AEs are shown in Figure 5. While errors in the predictions for each process variable had the same weights in the same in the loss function for this study, the errors could be weighted differently to prioritize accuracy in process variables known *a priori* to be more important or difficult to model.

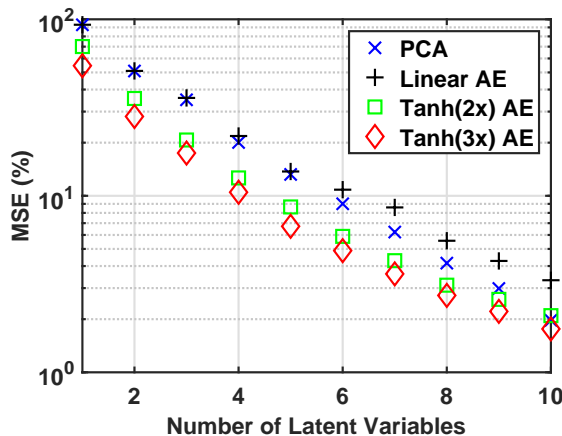


Figure 5: Comparison of validation MSE from dimensionality reduction techniques on process variables. The plotted MSEs were computed with 5-fold cross validation.

The results confirm the observation from the initial principal component analysis, that the closed-loop process dynamics can be “collapsed” to a lower dimension. For example, with ten dimensions, the tested methods can represent the complete input data very well, with MSEs around 2%. PCA presents an adequate manifold learning baseline for this simple process, but the nonlinear AEs perform better, especially at lower allowed dimensionality. The nonlinear AEs are capable of learning more complex relationships present in the data⁴⁶, and the increase from one hidden layer to two layers further increases representation power. The benefit of nonlinear mappings diminishes as the number of latent variables increases. Linear AEs operate in the same space as PCA⁶¹ and can theoretically learn an embedding with the same accuracy; however, we found that the accuracy of linear AEs to be lower than PCA when the number of latent variables included was large. This deviation can be attributed to difficulty in training a large AE using a stochastic optimization procedure, while PCA computes the optimal solution analytically.

4.3.1 Effect of Measurement Noise

Dimensionality-reduction techniques are often employed for their ability to filter noisy data. Autoencoders in particular are often used to “de-noise” data, and noise is sometimes even artificially introduced during model training to improve generalization ability⁶¹. By constraining the intrinsic dimensionality of the retained information, latent variables retain the most important dynamics and can naturally filter measurement noise. Measurement noise was simulated by adding 5% normally distributed error to all process variables in the training data set. AEs with the same configurations as described above were trained, and the MSEs are shown in Figure 6. Similar to the cases without measurement noise (Figure 5), the nonlinear AEs provide better process representations when the desired dimensionality is low, and the benefits of a nonlinear model decrease as more latent variables

are added. All models are less accurate when measurement noise is added, but we believe that this accuracy could be improved by increasing the size of the data set.

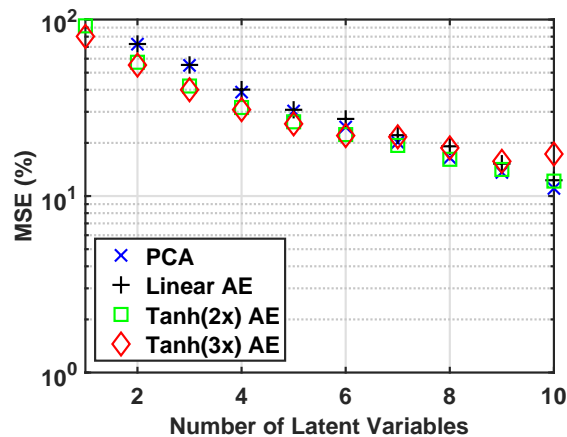


Figure 6: Comparison of validation MSE from dimensionality reduction techniques with 5% normally distributed measurement noise. The plotted MSEs were computed with 5-fold cross validation.

Insight into the denoising ability of the learned models can be obtained from examining their accuracy against the “ground truth” data (i.e., the data without measurement noise). The MSEs of the models shown in Figure 6 evaluated against the ground truth data are shown in Figure 7. The MSEs decrease rapidly as the number of latent variables increases from one to six, where the model accuracy plateaus at approximately 15% MSE. Interestingly, the learned models are generally more accurate against the ground truth data than the noisy data, demonstrating their ability to filter noise. Nevertheless, the MSEs in Figure 7 are higher than those computed with no error (Figure 5), showing that the measurement noise limits the maximum possible information gleaned from the data set. Since least-squares regression filters progressively more Gaussian noise as the number of samples increases, we again expect that the model accuracies could be improved by increasing the size of the data set.

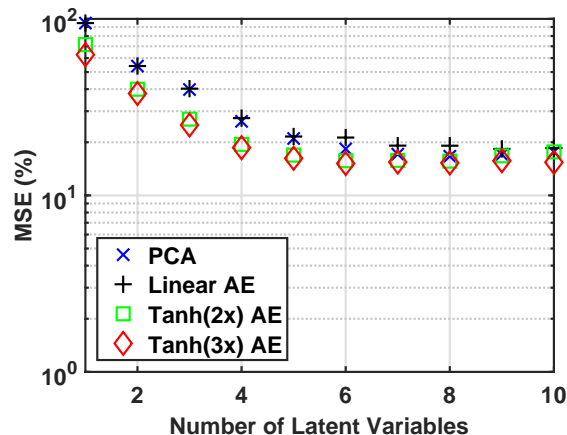


Figure 7: Comparison of validation MSE computed against “ground truth” from dimensionality reduction techniques with 5% normally distributed measurement noise. The plotted MSEs were computed with 5-fold cross validation.

4.3.2 Effect of Additional Process Variables

To confirm that the low-order manifold mapping for \mathbf{x}^* is not enabled by coincidentally selecting 15 correlated variables, the same AEs were trained on the full \mathbf{x}^* vector that includes all 70 *process-level* variables, as described in Section 4.2. The cross-validated test MSEs from training the AEs on the full vector of process-wide variables are shown in Figure 8. The dimension of the hidden layers in the nonlinear AEs was again chosen to be the truncated average between the input layer and latent variable dimensions. The AEs were implemented and trained using the same procedure as above. Note that the AEs have more units (and representation power) due to the increase in dimension of the input layer.

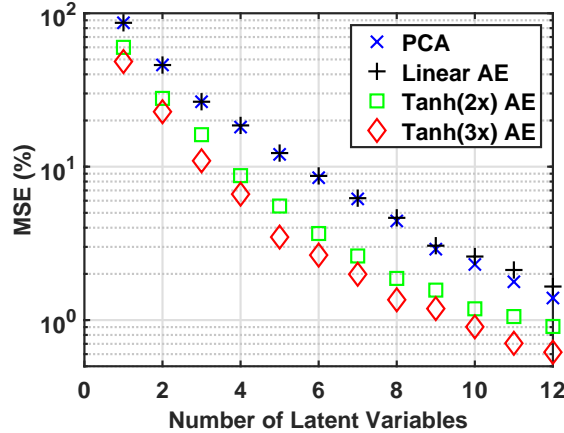


Figure 8: Comparison of validation MSE from dimensionality reduction techniques on all 70 process-level variables. The plotted MSEs were computed with 5-fold cross validation.

As expected, increasing the dimension of \mathbf{x}^* does not have a significant effect on the manifold learning procedure, since the intrinsic dimension $\dim_i(\mathbf{x}^*)$ remains unchanged. This result supports the assertion that the dimensionality reduction is enabled by the low intrinsic dimension of the system. We again find that the closed-loop process dynamics of all 70 variables can be “collapsed” to a low dimension, with each additional dimension having a diminishing impact on model accuracy. The linear AE again exhibits a similar result to performing PCA on the data set, while the nonlinear AEs again perform better than both linear methods. The nonlinear AEs show improved accuracy compared to Figure 5 since they have more hidden units. The MSEs for the nonlinear AEs reach $\sim 1\%$ with ten latent variables, while the linear models reach MSEs of around 2%.

4.4 Dynamic Modeling Results

Given the low MSEs possible with increasing p , we expect system identification to be the limiting factor in model accuracy for this study. Pattison et al.²⁶ found that a 10% “back-off” constraint was needed to compute feasible schedules for the ASU with HW models of physical variables, providing insight into SBM accuracy. We therefore select two low-dimensional representations of the ASU process dynamics with approximately 10% MSE (Figure 5): a linear AE with six latent variables and a nonlinear AE with one hidden layer and five latent variables. To investigate the effect of adjusting p we also test two representations with approximately 20% MSE: a linear AE with four latent variables and a nonlinear AE with one hidden layer and three latent variables. For dynamic system identification, the first 18 days were used as training data (90% of the data set). The process variables \mathbf{x}^* were encoded using the respective encoders to give $\phi = c(\mathbf{x}^*)$; $\phi \in \mathbb{R}^p$. The remaining two days are shown as dashed lines in Figure 3 and were left as test data. The test data were generated using electricity price data from a month not included in the training

data to account for the potential for unforeseen patterns in the production schedules. The effect of dimensionality reduction on the test data was evaluated as a baseline by computing their estimated values $\mathbf{x}^{*l} = c^{inv}(\phi)$ using the true values of $\phi = c(\mathbf{x}^*)$. The profiles of the variables \mathbf{x}^* as well as their estimated values using all four AEs are shown in Figure 9.

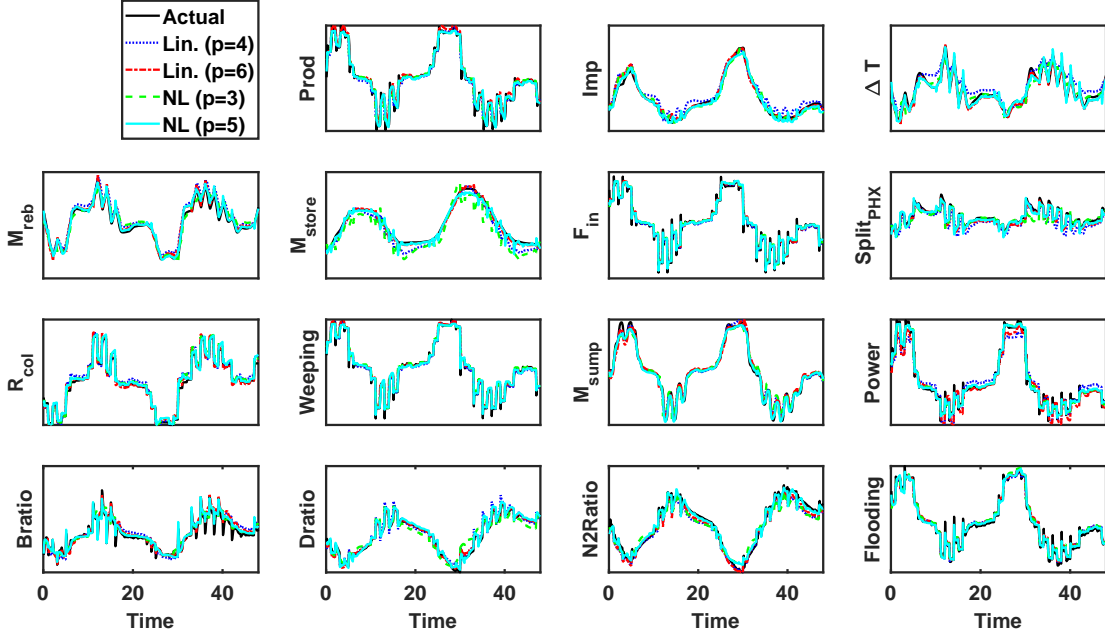


Figure 9: Evolution of the process variables predicted using various reduced-order representations, given “true” values of the latent variables.

Similar to our previous works^{26;30}, Hammerstein-Wiener (HW) models were fitted to process dynamics. However, the identified dynamics here refer to the dynamics of the *latent* variables of the process $\dot{\phi}_i = f_i^\phi(\phi_i, \mathbf{y}_{sp})$. The models were fitted using the System Identification Toolbox in MATLAB⁶⁴. Piecewise-linear and polynomial transformations were used to model the H and W blocks of (18)–(21). The form and polynomial order/number of piecewise segments for each transformation was determined by minimizing the normalized Akaike information criterion (nAIC) while using a large number of piecewise-linear segments for the other transformations and a high-order linear state-space model. The order of each linear state-space model was similarly determined using the nAIC. The resulting HW model structures and normalized mean squared error (NMSE) are shown in Tables 2 and 3. Note that a higher NMSE indicates a better fit, in contrast to MSE. The models for the nonlinear latent variables are slightly less accurate, suggesting that the nonlinear latent variables may exhibit more complex dynamics. The NMSE values are computed using the `goodnessOfFit()` function in MATLAB, which uses the following formula:

$$\text{NMSE} = 1 - \frac{\|x_{ref} - x\|^2}{\|x_{ref} - \text{mean}(x_{ref})\|^2} \quad (23)$$

The latent variable HW models were then simulated with the respective decoder $c^{inv}(\cdot)$ (created during autoencoder training) incorporated as additional static equalities. The simulations provide estimates of the latent variables ϕ and decoded estimates of the process variables $\mathbf{x}^{*l} = c^{inv}(\phi)$. The actual variable profiles \mathbf{x}^* and the estimated process variable profiles $\mathbf{x}^{*l}(t)$ are shown in Figure

Variable	Linear ($p = 4$)				Linear ($p = 6$)			
	H		W		H		W	
	Form	n_d	Form	NMSE train/test	Form	n_d	Form	NMSE train/test
ϕ_1	pwl-1	4	poly-2	0.77/0.78	pwl-3	5	pwl-2	0.83/0.86
ϕ_2	pwl-2	4	pwl-1	0.78/0.88	pwl-1	6	pwl-3	0.72/0.74
ϕ_3	pwl-2	5	pwl-1	0.93/0.96	pwl-1	4	poly-2	0.90/0.93
ϕ_4	pwl-2	5	poly-2	0.54/0.51	pwl-4	4	pwl-4	0.70/0.79
ϕ_5	-	-	-	-	poly-2	4	pwl-3	0.85/0.90
ϕ_6	-	-	-	-	pwl-4	4	pwl-5	0.64/0.63
average	-	-	-	0.76/0.78	-	-	-	0.77/0.81

Table 2: Hammerstein-Wiener model structures and accuracies for linear latent variables. Nonlinear transformations are denoted with ‘pwl’ for piecewise-linear and ‘poly’ for polynomial.

Variable	Nonlinear ($p = 3$)				Nonlinear ($p = 5$)			
	H		W		H		W	
	Form	n_d	Form	NMSE train/test	Form	n_d	Form	NMSE train/test
ϕ_1	pwl-3	5	pwl-3	0.76/0.83	pwl-5	8	pwl-2	0.49/0.38
ϕ_2	pwl-4	4	pwl-2	0.77/0.89	poly-2	8	pwl-1	0.74/0.83
ϕ_3	pwl-3	6	poly-3	0.53/0.70	pwl-2	4	poly-3	0.89/0.90
ϕ_4	-	-	-	-	pwl-3	4	pwl-3	0.69/0.83
ϕ_5	-	-	-	-	pwl-2	5	pwl-2	0.70/0.77
average	-	-	-	0.69/0.81	-	-	-	0.70/0.74

Table 3: Hammerstein-Wiener model structures and accuracies for nonlinear latent variables. Nonlinear transformations are denoted with ‘pwl’ for piecewise-linear and ‘poly’ for polynomial.

10. The NMSEs for all 15 variables are shown in Table 4. While the SBMs for the latent variables exhibited lower NMSEs (Tables 2 and 3), the final predictions for the process variables have NMSEs (Table 4) comparable to (or even higher than) previous works. Pattison et al.²⁶ reported an average validation NMSE of 83.75% using HW models to directly represent the behavior of eight physical variables. The study²⁶ employed heuristic controllers rather than MPC.

The agreement between the actual values and the estimated profiles is generally very good, confirming the closed-loop process dynamics are approximated well by a data-driven model whose dynamics are confined to a low-dimensional, intrinsic manifold. The NMSEs are slightly lower than those found in our previous work²⁶ by carrying out system identification for the evolution of the *physical* variables of the same process. There are two main reasons for this: (i) in the current work, prediction error arises both from the latent variable SBMs and the low-dimensional approximation, and (ii) the current work includes MPC operating on a 6-minute time interval, which is faster than changes in \mathbf{y}_{sp} . Since \mathbf{y}_{sp} changes on an hourly interval in response to electricity price, faster dynamics in \mathbf{x}^* may not be modeled well by the SBM. As expected, increasing the dimensionality of the latent manifold from four to six in the linear case, and from three to five in the nonlinear case, improves the accuracy of the model predictions. The predictions of the integrated reboiler-condenser temperature difference ΔT_{IRC} and the PHX split fraction suffer from the largest inaccuracy. The predictions are slightly improved by increasing dimensionality, but a comparison between Figures 9 and 10 suggests that the error is primarily introduced by the system identification step.

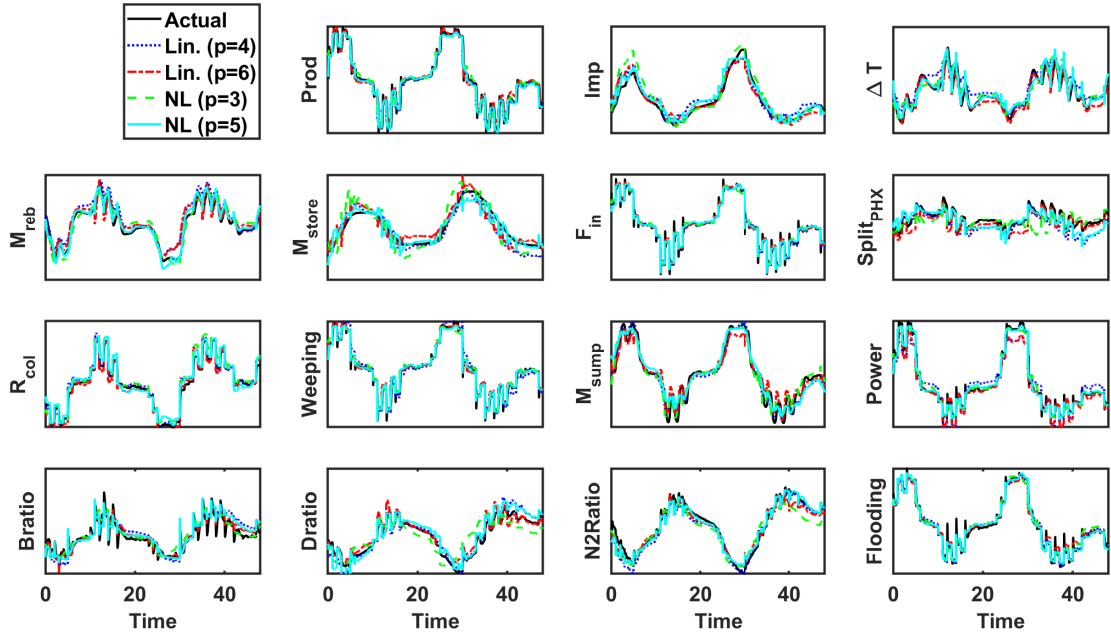


Figure 10: Evolution of the process variables predicted using various reduced-order representations, given values for the latent variables predicted by the identified HW models.

Variable	NMSE			
	Lin ($p = 4$)	Lin ($p = 6$)	NL ($p = 3$)	NL($p = 5$)
Production	0.95	0.96	0.95	0.97
Impurity	0.92	0.91	0.81	0.93
ΔT_{IRC}	0.63	0.90	0.68	0.86
M_{reb}	0.83	0.89	0.86	0.94
M_{store}	0.86	0.85	0.71	0.90
Air Flow	0.98	0.98	0.98	0.97
PHX Split	0.21	0.52	0.10	0.31
R_{col}	0.96	0.95	0.94	0.95
Weeping Ratio	0.96	0.97	0.97	0.98
Sump Level	0.95	0.94	0.93	0.93
Power	0.91	0.94	0.97	0.98
B Ratio	0.71	0.88	0.80	0.77
D Ratio	0.89	0.91	0.70	0.86
N_2 Ratio	0.93	0.95	0.87	0.96
Flooding Ratio	0.98	0.97	0.97	0.98
Average	0.85	0.90	0.83	0.89

Table 4: NMSEs found on validation data set with linear (Lin) and nonlinear (NL) autoencoders at various levels of dimensionality reduction. Values below 0.75 are in bold.

4.5 Optimal Scheduling Results

To verify the application of the proposed framework to the ASE demand-response integrated scheduling and control problem, the latent-variable scheduling optimization problem (12)–(16) was

Case	Cost	Difference from baseline	Solution time
Baseline ^a	\$707.91	0%	-
Previous work ^b	\$698.30	1.4%	381s
Lin. ($p = 4$)	\$700.75	1.0%	104s
Lin. ($p = 6$)	\$699.89	1.1%	113s
NL ($p = 3$)	\$701.65	0.9%	193s
NL ($p = 5$)	\$700.09	1.1%	238s

^a Baseline denotes the constant production rate case

^b Optimal point found using a simulation-optimization framework by²⁵. Only variables involved in the MPC were modeled and constrained during optimization.

Table 5: Optimal schedule economic results

solved for the demand response operational scenario considered by Dias et al.²⁵. In this scenario, the storage tank is assumed to have a maximum capacity of 200 kmol of liquid nitrogen, with an initial inventory of 50 kmol. The inventory must be returned to at least its initial value at the end of the scheduling horizon to eliminate the potential of reporting false economic benefits derived from selling pre-existing inventory. The day-ahead electricity prices are assumed to be known over a 48-hour horizon, and there is a constant demand of 20 mol/s for the gas nitrogen product (equal to the nominal capacity of the plant). We consider here only the “offline” scheduling problem (with no re-scheduling); however, the proposed framework allows the scheduling problem to be solved quickly (~ 100 -200s), which may benefit online scheduling techniques in the future^{27;13}.

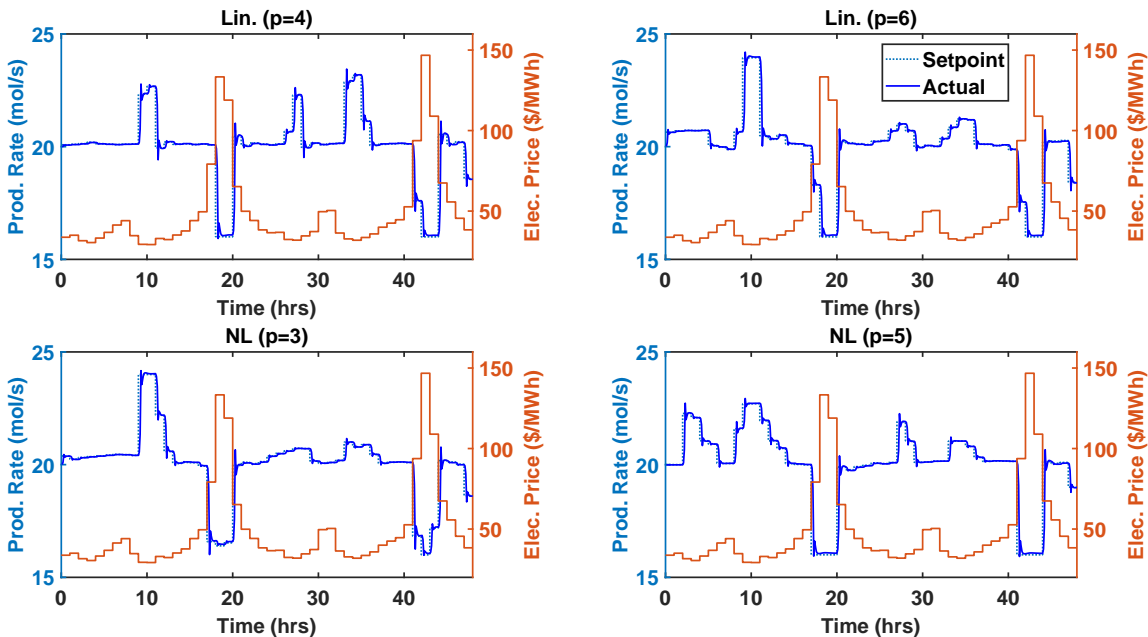


Figure 11: Optimal schedules and electricity prices.

4.5.1 Linear Mappings

The 48-hr scheduling problem was solved with the proposed latent-variable approach, using the linear mappings with $p = 4$ and $p = 6$. The models were implemented in gPROMS⁷², and opti-

mization was carried out using the built-in sequential dynamic optimization solver. The presented optimal points represent local optima found using 20 mol/s as the initial guess for the production setpoint at all times. The calculations were performed on a 64-bit Windows system with Intel Core i7-8700 CPU at 3.20 GHz and 16GB RAM. The implementation with four linear latent variables includes 29 differential variables and 64 total variables, while that with six linear latent variables includes 38 differential variables and 79 total variables. The scheduling problem with four latent variables was solved in 52 iterations, using 104.7s of CPU time (2.0s per iteration). The problem with six latent variables was solved in 42 iterations, using 113.0s of CPU time (2.7s per iteration). The two optimal schedules were simulated using the full-order dynamic model.

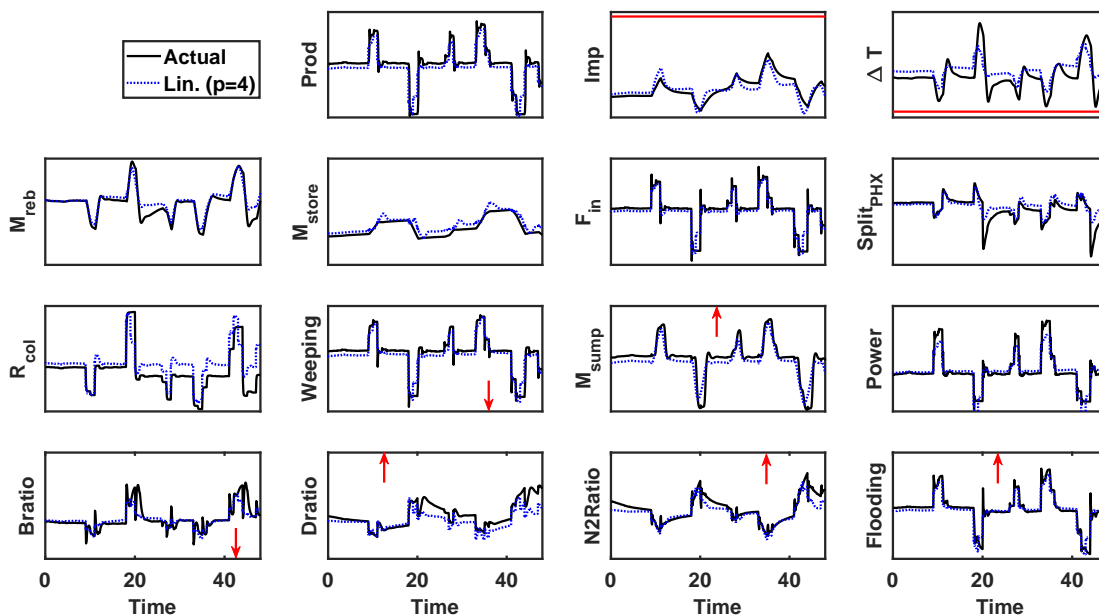


Figure 12: Optimal schedule generated with linear AEs ($p=4$). “Actual” profiles are generated by simulation of the full-order model with online MPC. Variable bounds are shown in red. Ordinate limits are 0-100% of the respective scaled variable. Some bounds/constraints do not appear within this scaling; their locations are indicated with an arrow.

The production rates found in simulation of the optimal schedules are shown in Figure 11, along with their setpoints/targets, which are closely tracked. As expected, production rates are scheduled to decrease when energy prices are high in both schedules. The behaviors of all 15 modeled process variables in the two computed schedules are shown in Figures 12 and 13. The temperature driving force across the reboiler/condenser nearly reaches its bound in both schedules, but this potential constraint violation is only predicted by the low-dimensional representation when six linear latent variables are included. None of the other variable path constraints were reached when the optimal schedules were simulated with the full-order dynamic model. The end point constraints of returning the storage and reboiler levels to at least their initial conditions were also met in both schedules. We note that although the variables with inactive constraints may not have been necessary for computing a feasible schedule, the proposed approach models the dynamics of all constrained variables in the scheduling problem. This eliminates the difficult task of anticipating which constraints may be violated and should therefore be modeled.

The predictions are generally improved by including six (vs. four) latent variables, especially

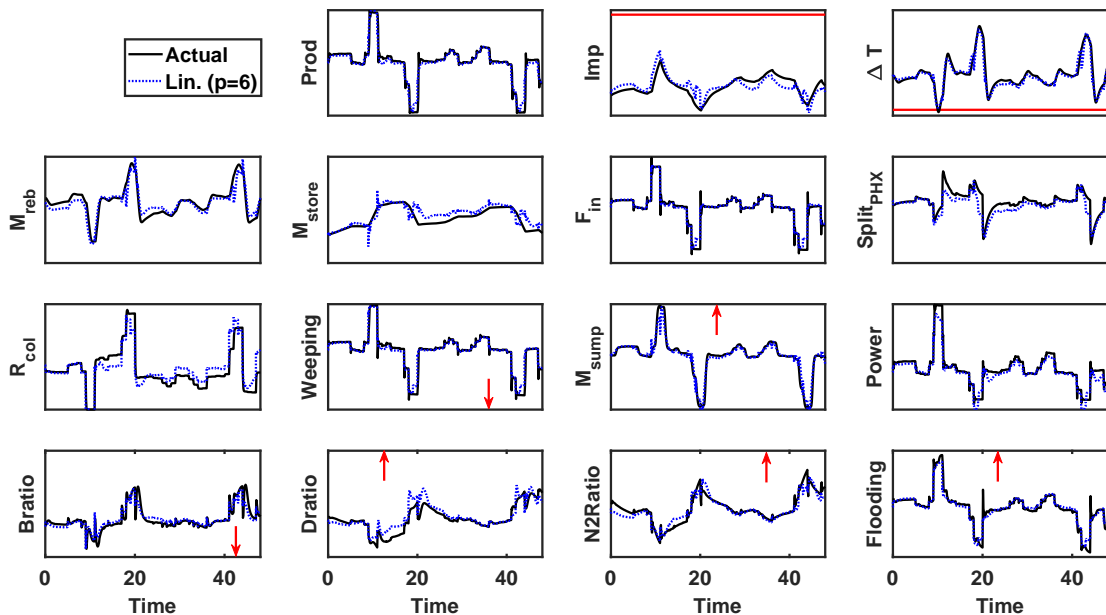


Figure 13: Optimal schedule generated with linear AEs ($p=6$). “Actual” profiles are generated by simulation of the full-order model with online MPC. Variable bounds are shown in red. Ordinate limits are 0-100% of the respective scaled variable. Some bounds/constraints do not appear within this scaling; their locations are indicated with an arrow.

in the aforementioned temperature driving force ΔT and PHX split fraction. However, some deviations are visible for the column reflux R_{col} predictions with both models (Figures 12 and 13). The operational costs calculated using the full-order dynamic model of the computed schedules are shown in Table 5. Both schedules result in a approximately 1% savings compared to a constant production profile set at the nominal rate (subject to the same electricity price profile). These savings are similar to those reported in²⁵ and represent a substantial amount in the context of the well-established, commoditized air separation industry. In contrast to the previous approaches, the proposed method maintains the computational efficiency of scheduling in a reduced dimension while providing predictions of all constrained variables.

4.5.2 Nonlinear Mappings

The same 48-hr latent-variable scheduling problem was solved using the nonlinear mappings with $p = 3$ and $p = 5$. The same implementation and optimization settings were used, but the models include a hidden layer and nonlinear transformations. The implementation with three nonlinear latent variables includes 25 differential variables and 66 total variables, while that with five nonlinear latent variables includes 38 differential variables and 86 total variables. The scheduling problem with three nonlinear latent variables was solved in 69 iterations, using 192.8s of CPU time (2.8s per iteration). The problem with five latent variables was solved in 61 iterations, using 237.8s of CPU time (3.9s per iteration). Although the problems with four linear and three nonlinear latent variables have similar numbers of variables, the optimization problems with nonlinear latent variables require more time per optimization iteration. The same phenomenon is observed for the problems with six linear and five nonlinear latent variables. The slowdown can be attributed to the nonlinear \tanh transformations limiting integration step sizes and thereby slowing down the implicit time-integration scheme at each iteration.

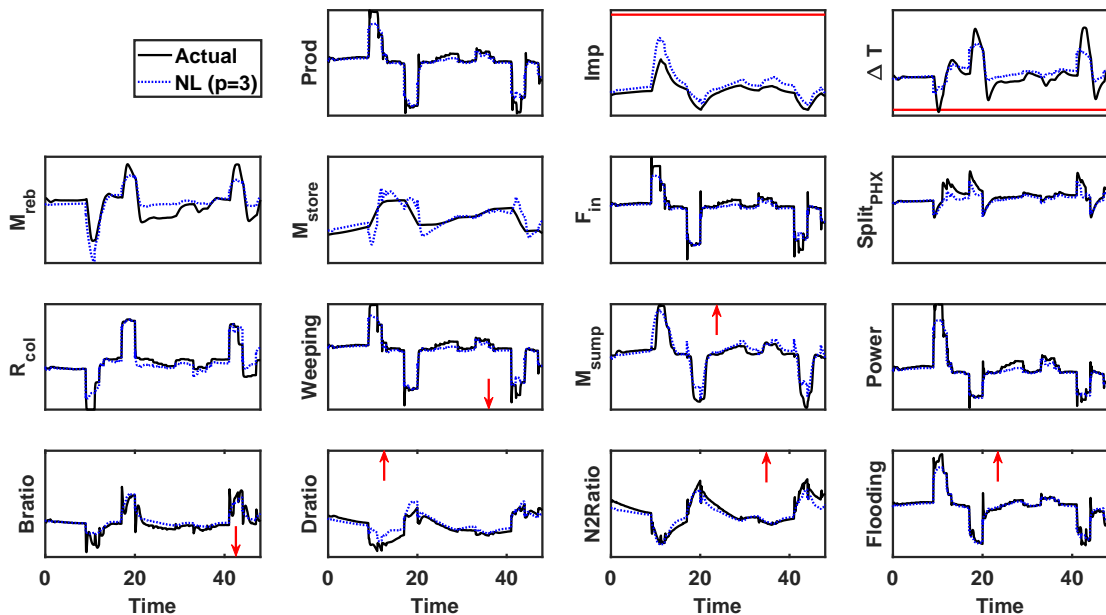


Figure 14: Optimal schedule generated with nonlinear AEs ($p=3$). “Actual” profiles are generated by simulation of the full-order model with online MPC. Variable bounds are shown in red. Ordinate limits are 0-100% of the respective scaled variable. Some bounds/constraints do not appear within this scaling; their locations are indicated with an arrow.

The two computed optimal schedules were simulated with the aforementioned MPC and the full-order dynamic model. The production rate setpoints and actual values found at the optimal points are again shown in Figure 11. The behavior of all 15 modeled process variables in the two computed schedules is shown in Figures 14 and 15. The temperature driving force across the reboiler/condenser slightly violates the respective bound in the schedule computed with three nonlinear latent variables, which is not predicted accurately by the reduced-order model. The end point constraints of returning the storage and reboiler levels to at least their initial conditions were met in both schedules.

The optimization problem with dynamics represented by five nonlinear latent variables demonstrates the most accurate predictions of the evolution of process variables, but also required the most time per optimization iteration out of the four tested latent-variable scheduling problems. However, the optimization problem size is still greatly reduced from previous approaches^{26;27;25}, and correspondingly, the optimal schedule was obtained with less computational effort. In addition, the proposed formulation allows for more information on the process dynamics to be captured in scheduling calculations, with all constrained process variables predicted relatively accurately. The results in Section 4.3.2 further suggest that more process-level variables could be easily included at similar levels of accuracy without increasing the size of the latent dynamics. The intrinsic, low-dimensional dynamics underlying the closed-loop system would be approximated, and the decoder could be expanded to include more process variables.

5 Conclusions

The integration of closed-loop process dynamics in production scheduling calculations is key to ensuring that production schedules do not violate process constraints when implemented in practice (i.e., the schedules are “dynamically feasible”). This is especially important when production

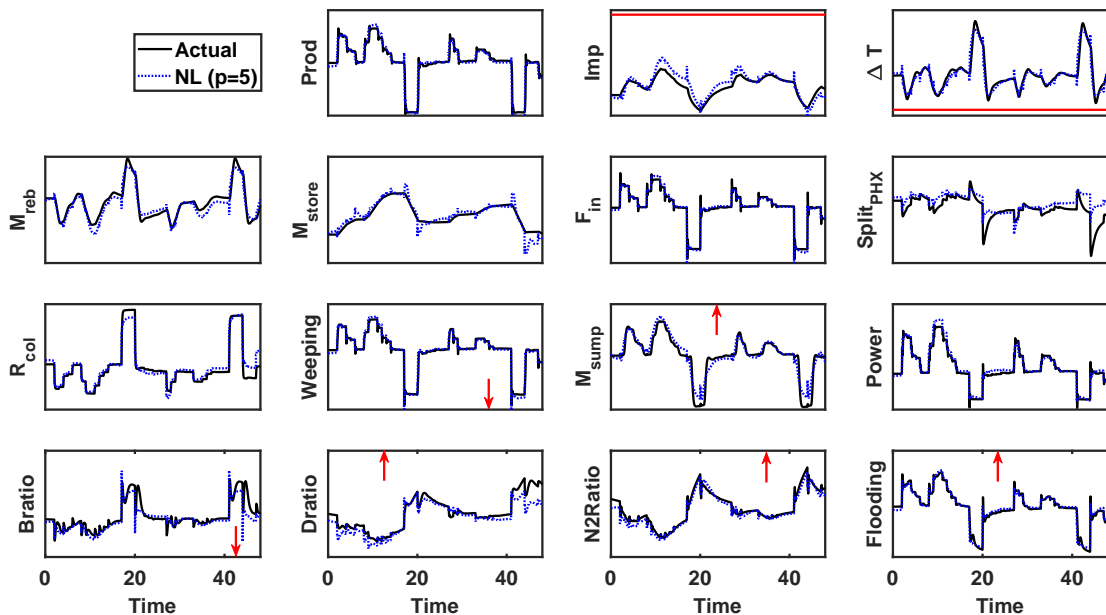


Figure 15: Optimal schedule generated with nonlinear AEs ($p=5$). “Actual” profiles are generated by simulation of the full-order model with online MPC. Variable bounds are shown in red. Ordinate limits are 0-100% of the respective scaled variable. Some bounds/constraints do not appear within this scaling; their locations are indicated with an arrow.

changes are frequent, such as in practical cases driven by fast-changing external conditions. However, there is an intrinsic tradeoff between the amount of dynamic information captured in the scheduling model and the computational complexity required for its optimization. Driven by the need for computationally efficient representations of process dynamics, we exploit the low intrinsic dimensionality of closed-loop process behavior to generate reduced-order models. We proposed a data-driven approach for learning a low-dimensional latent manifold underlying variations in recorded observations, which can then be used to represent the process behavior. We present a conceptual analysis of the existence of such a manifold, and we demonstrate the means for selecting the dimensionality of the latent manifold, so as to balance between complexity of the captured dynamics and model size.

We present a framework for production scheduling using the latent variable representation of process dynamics. In the proposed framework, process operating data are projected onto the latent manifold, and system identification and scheduling calculations are both performed in the latent variable space. Using this method, system identification is only necessary for a lower number of (latent) variables, and the scheduling calculations require less computational expense. These combined advantages allow for a broad complement of process variables to be modeled efficiently, and for the integrated scheduling and control problem to be solved in practically-relevant amounts of time. Notably, this approach eliminates the need for heuristically selecting variables to be modeled in scheduling calculations by automating the dimensionality reduction step. The framework was applied to the scheduling of an air separation unit under MPC in response to an hourly electricity price signal. The results confirm that the latent-variable scheduling formulation can retain more information about the process dynamics, compared to previous works, and simultaneously reduce the required computational effort.

6 Disclaimer

This report was prepared as an account of work sponsored by an agency of the United States Government. Neither the United States Government nor any agency thereof, nor any of their employees, makes any warranty, express or implied, or assumes any legal liability or responsibility for the accuracy, completeness, or usefulness of any information, apparatus, product, or process disclosed, or represents that its use would not infringe privately owned rights. Reference herein to any specific commercial product, process, or service by trade name, trademark, manufacturer, or otherwise does not necessarily constitute or imply its endorsement, recommendation, or favoring by the United States Government or any agency thereof. The views and opinions of authors expressed herein do not necessarily state or reflect those of the United States Government or any agency thereof.

7 Acknowledgements

The authors acknowledge funding from the National Science Foundation (NSF) through CAREER Award 1454433 and Award CBET-1512379. This material is also based on work supported by the US Department of Energy under Award Number de-oe0000841. CT thanks The University of Texas at Austin for support through the University Graduate Continuing Fellowship.

Literature Cited

1. Qi Zhang, Ignacio E Grossmann, Clara F Heuberger, Arul Sundaramoorthy, and Jose M Pinto. Air separation with cryogenic energy storage: optimal scheduling considering electric energy and reserve markets. *AIChE Journal*, 61(5):1547–1558, 2015.
2. Sebastian Engell and Iiro Harjunoski. Optimal operation: Scheduling, advanced control and their integration. *Computers & Chemical Engineering*, 47:121–133, 2012.
3. Michael Baldea and Iiro Harjunoski. Integrated production scheduling and process control: A systematic review. *Computers & Chemical Engineering*, 71:377–390, 2014.
4. Prodromos Daoutidis, Jay H Lee, Iiro Harjunoski, Sigurd Skogestad, Michael Baldea, and Christos Georgakis. Integrating operations and control: A perspective and roadmap for future research. *Computers & Chemical Engineering*, 115:179–184, 2018.
5. Lisia S Dias and Marianthi G Ierapetritou. Optimal operation and control of intensified processes—challenges and opportunities. *Current Opinion in Chemical Engineering*, 2019. doi:10.1016/j.coche.2018.12.008.
6. Alexander W Dowling, Ranjeet Kumar, and Victor M Zavala. A multi-scale optimization framework for electricity market participation. *Applied Energy*, 190:147–164, 2017.
7. Joannah I Otashu and Michael Baldea. Grid-level battery operation of chemical processes and demand-side participation in short-term electricity markets. *Applied Energy*, 220:562–575, 2018.
8. Pascal Schäfer, Hermann Graf Westerholt, Artur M Schweidtmann, Svetlina Ilieva, and Alexander Mitsos. Model-based bidding strategies on the primary balancing market for energy-intensive processes. *Computers & Chemical Engineering*, 120:4–14, 2019.
9. S Joe Qin and Thomas A Badgwell. A survey of industrial model predictive control technology. *Control Engineering Practice*, 11(7):733–764, 2003.
10. Antonio Flores-Tlacuahuac and Ignacio E Grossmann. Simultaneous cyclic scheduling and control of a multiproduct CSTR. *Industrial & Engineering Chemistry Research*, 45(20):6698–6712, 2006.
11. Jinjun Zhuge and Marianthi G Ierapetritou. Integration of scheduling and control with closed loop implementation. *Industrial & Engineering Chemistry Research*, 51(25):8550–8565, 2012.
12. Logan DR Beal, Damon Petersen, David Grimsman, Sean Warnick, and John D Hedengren. Integrated scheduling and control in discrete-time with dynamic parameters and constraints. *Computers & Chemical Engineering*, 115:361–376, 2018.
13. Logan Beal, Damon Petersen, Guilherme Pila, Brady Davis, Sean Warnick, and John Hedengren. Economic benefit from progressive integration of scheduling and control for continuous chemical processes. *Processes*, 5(4):84, 2017.
14. Robert W Koller, Luis A Ricardez-Sandoval, and Lorenz T Biegler. Stochastic back-off algorithm for simultaneous design, control, and scheduling of multiproduct systems under uncertainty. *AIChE Journal*, 64(7):2379–2389, 2018.
15. Rasmus H Nyström, Rüdiger Franke, Iiro Harjunoski, and Andreas Kroll. Production campaign planning including grade transition sequencing and dynamic optimization. *Computers & Chemical Engineering*, 29(10):2163–2179, 2005.
16. Yisu Nie, Lorenz T Biegler, Carlos M Villa, and John M Wassick. Discrete time formulation for the integration of scheduling and dynamic optimization. *Industrial & Engineering Chemistry Research*, 54(16):4303–4315, 2014.

17. Jodie M Simkoff and Michael Baldea. Production scheduling and linear MPC: complete integration via complementarity conditions. *Computers & Chemical Engineering*, 2019. doi:10.1016/j.compchemeng.2019.01.024.
18. Baris Burnak, Justin Katz, Nikolaos A Diangelakis, and Efstratios N Pistikopoulos. Simultaneous process scheduling and control: A multiparametric programming-based approach. *Industrial & Engineering Chemistry Research*, 57(11):3963–3976, 2018.
19. Jinjun Zhuge and Marianthi G Ierapetritou. Integration of scheduling and control for batch processes using multi-parametric model predictive control. *AIChE Journal*, 60(9):3169–3183, 2014.
20. Vassilis M Charitopoulos, Lazaros G Papageorgiou, and Vivek Dua. Closed-loop integration of planning, scheduling and multi-parametric nonlinear control. *Computers & Chemical Engineering*, 2018.
21. Yanan Cao, Christopher LE Swartz, Jesus Flores-Cerrillo, and Jingran Ma. Dynamic modeling and collocation-based model reduction of cryogenic air separation units. *AIChE Journal*, 62(5):1602–1615, 2016.
22. Pascal Schäfer, Adrian Caspari, Kerstin Kleinhans, Adel Mhamdi, and Alexander Mitsos. Reduced dynamic modeling approach for rectification columns based on compartmentalization and artificial neural networks. *AIChE Journal*, 2019. doi:10.1002/aic.16568.
23. Juan Du, Jungup Park, Iiro Harjunoski, and Michael Baldea. A time scale-bridging approach for integrating production scheduling and process control. *Computers & Chemical Engineering*, 79:59–69, 2015.
24. Michael Baldea, Juan Du, Jungup Park, and Iiro Harjunoski. Integrated production scheduling and model predictive control of continuous processes. *AIChE Journal*, 61(12):4179–4190, 2015.
25. Lisia S Dias, Richard C Pattison, Calvin Tsay, Michael Baldea, and Marianthi G Ierapetritou. A simulation-based optimization framework for integrating scheduling and model predictive control, and its application to air separation units. *Computers & Chemical Engineering*, 113:139–151, 2018.
26. Richard C Pattison, Cara R Touretzky, Ted Johansson, Iiro Harjunoski, and Michael Baldea. Optimal process operations in fast-changing electricity markets: framework for scheduling with low-order dynamic models and an air separation application. *Industrial & Engineering Chemistry Research*, 55(16):4562–4584, 2016.
27. Richard C Pattison, Cara R Touretzky, Iiro Harjunoski, and Michael Baldea. Moving horizon closed-loop production scheduling using dynamic process models. *AIChE Journal*, 63(2):639–651, 2017.
28. Morgan T Kelley, Richard C Pattison, Ross Baldick, and Michael Baldea. An MILP framework for optimizing demand response operation of air separation units. *Applied Energy*, 222:951–966, 2018.
29. Calvin Tsay, Michael Baldea, Jun Shi, Ankur Kumar, and Jesus Flores-Cerrillo. Data-driven models and algorithms for demand response scheduling of air separation units. In G. P. Towler M. R. Eden, M. G. Ierapetritou, editor, *Computer Aided Chemical Engineering*, volume 44, pages 1273–1278, Proceedings of the 13th International Symposium on Process Systems Engineering, San Diego, CA, 2018. Elsevier.
30. Calvin Tsay, Ankur Kumar, Jesus Fores-Cerrillo, and Michael Baldea. Optimal demand response scheduling of an industrial air separation unit using data-driven dynamic models. *Computers & Chemical Engineering*, 2019. doi:10.1016/j.compchemeng.2019.03.022.
31. Michael Baldea and Prodromos Daoutidis. *Dynamics and nonlinear control of integrated process systems*. Cambridge University Press, Cambridge, United Kingdom, 2012.
32. Aditya Kumar, Panagiotis D Christofides, and Prodromos Daoutidis. Singular perturbation modeling of nonlinear processes with nonexplicit time-scale multiplicity. *Chemical Engineering Science*, 53(8):1491–1504, 1998.

33. Mingzhao Yu, David C Miller, and Lorenz T Biegler. Dynamic reduced order models for simulating bubbling fluidized bed adsorbers. *Industrial & Engineering Chemistry Research*, 54(27):6959–6974, 2015.
34. Mingzhao Yu and Lorenz T Biegler. A stable and robust nmPC strategy with reduced models and nonuniform grids. *IFAC-PapersOnLine*, 49(7):31–36, 2016.
35. Juergen Hahn and Thomas F Edgar. An improved method for nonlinear model reduction using balancing of empirical gramians. *Computers & Chemical Engineering*, 26(10):1379–1397, 2002.
36. Karen Willcox and Jaime Peraire. Balanced model reduction via the proper orthogonal decomposition. *AIAA Journal*, 40(11):2323–2330, 2002.
37. Antonios Armaou and Panagiotis D Christofides. Dynamic optimization of dissipative PDE systems using nonlinear order reduction. *Chemical Engineering Science*, 57(24):5083–5114, 2002.
38. Stefan Klus, Feliks Nüske, Péter Koltai, Hao Wu, Ioannis Kevrekidis, Christof Schütte, and Frank Noé. Data-driven model reduction and transfer operator approximation. *Journal of Nonlinear Science*, 28(3):985–1010, 2018.
39. Yucai Zhu. *Multivariable system identification for process control*. Elsevier Science, Oxford, United Kingdom, 2001.
40. Karl Pearson. LIII. on lines and planes of closest fit to systems of points in space. *The London, Edinburgh, and Dublin Philosophical Magazine and Journal of Science*, 2(11):559–572, 1901.
41. John F MacGregor, Honglu Yu, Salvador García Muñoz, and Jesus Flores-Cerrillo. Data-based latent variable methods for process analysis, monitoring and control. *Computers & Chemical Engineering*, 29(6):1217–1223, 2005.
42. Jesus Flores-Cerrillo and John F MacGregor. Latent variable MPC for trajectory tracking in batch processes. *Journal of Process Control*, 15(6):651–663, 2005.
43. D Laurí, JA Rossiter, J Sanchis, and M Martínez. Data-driven latent-variable model-based predictive control for continuous processes. *Journal of Process Control*, 20(10):1207–1219, 2010.
44. Bernhard Schölkopf, Alexander Smola, and Klaus-Robert Müller. Kernel principal component analysis. In *International Conference on Artificial Neural Networks*, pages 583–588. Springer, 1997.
45. Terence D Sanger. Optimal unsupervised learning in a single-layer linear feedforward neural network. *Neural networks*, 2(6):459–473, 1989.
46. Mark A Kramer. Nonlinear principal component analysis using autoassociative neural networks. *AIChE Journal*, 37(2):233–243, 1991.
47. Ronald R Coifman and Stéphane Lafon. Diffusion maps. *Applied and Computational Harmonic Analysis*, 21(1):5–30, 2006.
48. Mikhail Belkin and Partha Niyogi. Laplacian eigenmaps for dimensionality reduction and data representation. *Neural Computation*, 15(6):1373–1396, 2003.
49. Sam T Roweis and Lawrence K Saul. Nonlinear dimensionality reduction by locally linear embedding. *Science*, 290(5500):2323–2326, 2000.
50. Geoffrey E Hinton and Sam T Roweis. Stochastic neighbor embedding. In *Advances in Neural Information Processing Systems*, pages 857–864, 2003.
51. Joshua B Tenenbaum, Vin De Silva, and John C Langford. A global geometric framework for nonlinear dimensionality reduction. *Science*, 290(5500):2319–2323, 2000.

52. John A Lee and Michel Verleysen. *Nonlinear dimensionality reduction*. Springer Science & Business Media, New York, NY, 2007.
53. Laurens Van Der Maaten, Eric Postma, and Jaap Van den Herik. Dimensionality reduction: a comparative review. *Journal of Machine Learning Research*, 10:66–71, 2009.
54. EN Pistikopoulos. Perspectives in multiparametric programming and explicit model predictive control. *AIChE Journal*, 55(8):1918–1925, 2009.
55. Robert J Lovelett, Felix Dietrich, Seungjoon Lee, and Ioannis G Kevrekidis. Some manifold learning considerations towards explicit model predictive control. *arXiv preprint arXiv:1812.01173*, 2018.
56. Andreas Obermeier, Christoph Windmeier, Erik Esche, and Jens-Uwe Repke. A discrete-time scheduling model for power-intensive processes taking fatigue of equipment into consideration. *Chemical Engineering Science*, 195:904–920, 2019.
57. Johannes Wiebe, Inês Cecílio, and Ruth Misener. Data-driven optimization of processes with degrading equipment. *Industrial & Engineering Chemistry Research*, 57(50):17177–17191, 2018.
58. Vassilios S Vassiliadis, Roger WH Sargent, and Costas C Pantelides. Solution of a class of multistage dynamic optimization problems. 1. Problems without path constraints. *Industrial & Engineering Chemistry Research*, 33(9):2111–2122, 1994.
59. Vassilios S Vassiliadis, Roger WH Sargent, and Costas C Pantelides. Solution of a class of multistage dynamic optimization problems. 2. Problems with path constraints. *Industrial & Engineering Chemistry Research*, 33(9):2123–2133, 1994.
60. Lorenz T Biegler. An overview of simultaneous strategies for dynamic optimization. *Chemical Engineering and Processing: Process Intensification*, 46(11):1043–1053, 2007.
61. Ian Goodfellow, Yoshua Bengio, and Aaron Courville. *Deep learning*. MIT Press, Cambridge, MA, 2016.
62. Kurt Hornik. Approximation capabilities of multilayer feedforward networks. *Neural Networks*, 4(2):251–257, 1991.
63. Geoffrey E Hinton and Ruslan R Salakhutdinov. Reducing the dimensionality of data with neural networks. *Science*, 313(5786):504–507, 2006.
64. MathWorks. MATLAB System Identification Toolbox. <https://www.mathworks.com/help/ident/> (Accessed March 27, 2019).
65. Qi Zhang, Arul Sundaramoorthy, Ignacio E Grossmann, and Jose M Pinto. A discrete-time scheduling model for continuous power-intensive process networks with various power contracts. *Computers & Chemical Engineering*, 84:382–393, 2016.
66. Danyan Zhou, Kai Zhou, Lingyu Zhu, Jun Zhao, Zuhua Xu, Zhijiang Shao, and Xi Chen. Optimal scheduling of multiple sets of air separation units with frequent load-change operation. *Separation and Purification Technology*, 172:178–191, 2017.
67. Shengnan Zhao, Maria Paz Ochoa, Lixin Tang, Irene Lotero, Ajit Gopalakrishnan, and Ignacio E Grossmann. Novel formulation for optimal schedule with demand side management in multi-product air separation processes. *Industrial & Engineering Chemistry Research*, 58(8):3104–3117, 2019.
68. Yanan Cao, Christopher LE Swartz, Michael Baldea, and Stéphane Blouin. Optimization-based assessment of design limitations to air separation plant agility in demand response scenarios. *Journal of Process Control*, 33:37–48, 2015.
69. Ted Johansson. Integrated scheduling and control of an air separation unit subject to time-varying electricity prices. Master’s thesis, KTH Royal Institute of Technology, Stockholm, Sweden, 2015.

70. Martín Abadi, Paul Barham, Jianmin Chen, Zhifeng Chen, Andy Davis, Jeffrey Dean, Matthieu Devin, Sanjay Ghemawat, Geoffrey Irving, Michael Isard, et al. Tensorflow: A system for large-scale machine learning. In *12th USENIX Symposium on Operating Systems Design and Implementation (OSDI 16)*, pages 265–283, 2016.
71. Diederik P Kingma and Jimmy Ba. Adam: A method for stochastic optimization. *arXiv preprint arXiv:1412.6980*, 2014.
72. Process Systems Enterprise. general PROcess Modeling System (gPROMS). www.psententerprise.com/gproms, 1997-2019.

Appendix

#	Variable	Description	Unit	This Work	Pattison et al. ²⁶	Dias et al. ²⁵
1	Prod	Production flow rate	mol/s	x	x	x
2	Imp	Product impurity	ppm	x	x	x
3	ΔT	Temperature difference in IRC	K	x	x	x
4	M_{reb}	Reboiler liquid level	mol	x	x	x
5	M_{store}	Storage liquid level	mol	x	x^a	x
6	F_{in}	Air flow in	mol/s	x	x	x
7	Split _{PHX}	PHX split fraction	%	x	-	x
8	R_{col}	Vapor product split	%	x	-	x
9	Weeping	Column weeping ratio	%	x	x	-
10	M_{sump}	Sump liquid level	mol	x	-	-
11	Power	Power consumption	MW	x	x^a	x
12	Bratio	PHX outlet P / bubble point P	%	x	x	-
13	Dratio	Turbine 1 inlet P / dew point P	%	x	x	-
14	N2ratio	Turbine 2 inlet P / dew point P	%	x	-	-
15	Flooding	Column flooding ratio	%	x	-	-

^aPattison et al.²⁶ leveraged process knowledge to estimate static models for the plant power consumption and storage level based on the production flow rate rather than create separate dynamic models.

Table A1: Variables dynamically modeled in ASU case study for various approaches.

#	Variable	unit	Lower Bound	Upper Bound	0% Scaled Value	100% Scaled Value
1	Prod	mol/s	-	-	15.81	24.17
2	Imp	ppm	-	1800	158.68	1872.73
3	ΔT	K	1.9	-	1.85	2.80
4	M_{reb}	mol	0	-	86148.62	109259.89
5	M_{store}	mol	0	-	0.00	161097.47
6	F_{in}	mol/s	-	-	30.41	49.62
7	Split _{PHX}	%	-	-	3.19	3.83
8	R_{col}	%	-	-	51.57	52.73
9	Weeping	%	105	-	1902.67	3025.24
10	M_{sump}	mol	0	5000	2002.46	2876.60
11	Power	MW	-	-	0.22	0.45
12	Bratio	%	105	-	163.13	183.22
13	Dratio	%	-	95	81.69	90.80
14	N2ratio	%	-	95	57.85	69.01
15	Flooding	%	-	95	68.68	96.57

Table A2: Scaled variable ranges and bounds for ASU case study. “Back-off” bounds are used to account for model inaccuracy.

Supporting Information

```
from tensorflow.keras.layers import Input, Dense
from tensorflow.keras.models import Model
from tensorflow.keras.optimizers import Adam, Nadam
import numpy as np

#location of dataset
#dataset should have size of [#samples+headersize, #dimensions]
headersize = 1
filename = 'data.csv'

#hyperparameters for autoencoder training
learning_rate = 0.01
num_epochs = 500
num_batch = 480
output_level = 0
encoding_dim = 5; #number of dimensions in the bottleneck layer

#split dataset into training and validation
X = np.genfromtxt(filename,delimiter=',',skip_header=headersize)
n = X.shape[1];
Xtrain = X[0:int(n*0.9),:]
Xval = X[int(n*0.9):,:]

#build autoencoder with one hidden layer on either side of bottleneck layer
inputlayer = Input(shape=(n,))
hidden1 = Dense(int(np.average([n,encoding_dim])), activation='tanh')(inputlayer)
encoded = Dense(encoding_dim, activation='tanh')(hidden1)
hidden2 = Dense(int(np.average([n,encoding_dim])), activation='tanh')(encoded)
decoded = Dense(n, activation='tanh')(hidden2)

#construct models using keras function API
autoencoder = Model(inputlayer, decoded)
encoder = Model(inputlayer,encoded)

#select optimizer and compile model
optimizer = Adam(lr=learning_rate)
autoencoder.compile(optimizer=optimizer, loss='mean_squared_error')

#train model
history = autoencoder.fit(X,X,epochs=num_epochs,batch_size=num_batch,
verbose=output_level,validation_data=(Xval,Xval))

#compute encoded data and decoded data
encoded_data = encoder.predict(X)
decoded_data = autoencoder.predict(X)
```

Figure S1: A simple Python script for training a nonlinear autoencoder with `tanh` activation functions using Tensorflow and its Keras high-level API. The last 10% of the data set is used as validation data.